Oxygen variability in the offshore northern Benguela Upwelling System from glider data

Elisa Lovecchio[1], Stephanie Henson[1], Filipa Carvalho[1], Nathan Briggs[1]

[1]National Oceanography Centre, European Way, Southampton, U.K.

Key Points:

- Alternating subsurface physical fluxes of Angola- and Benguela-derived waters drive mesopelagic oxygen variability in the offshore Benguela
- Hypoxic events ($O_2 < 60$ µmol) are intermittent and are associated with weekly pulses of tropical water in the upper mesopelagic
- Mesoscale eddies further modulate the oxygen field and are associated with severe hypoxia, fine-scale oxygen patchiness and water mass mixing

Corresponding author: Elisa Lovecchio, elisa.lovecchio@noc.ac.uk

This article has been accepted for publication and undergone full peer review but has not been through the copyediting, typesetting, pagination and proofreading process, which may lead to differences between this version and the Version of Record. Please cite this article as doi: 10.1029/2022JC019063.

Abstract

Despite their role in modulating the marine ecosystem, variability and drivers of low-oxygen events in the offshore northern Benguela Upwelling System (BenUS) have been rarely investigated due to the events' episodicity which is difficult to resolve using shipboard measurements. We address this issue using 4 months of high-resolution glider data collected between February and June 2018, 100 km offshore at 18 °S. We find that oxygen concentrations in the offshore northern Benguela are determined by the subsurface alternation of low-oxygen Angola-derived water and oxygenated water from the south at 100 - 500 m depth. We observe intermittent hypoxia ($O_2 < 60$ µmol kg^{-1}) which occurs on average for ∼30 % of the 4 month deployment and is driven by the time-varying subsurface pulses of Angola-derived tropical water. Hypoxic events are rather persistent at depths of 300 - 450 m, while they are more sporadic and have weekly duration at shallower depths (100 - 300 m). We find extreme values of hypoxia, with O_2 minima of 16 µmol kg^{-1}, associated with an anticyclonic eddy spinning from the undercurrent flowing on the BenUS shelf and showing no surface signature. Fine-scale patchiness and water mass mixing are associated with cross-frontal stirring by a large anticyclone recirculating tropical water into the northern BenUS. The dominance of physical drivers and their high variability on short time scales reveal a dynamic coupling between Angola and Benguela, calling for long-term and high-resolution measurements and studies focusing on future changes of both tropical oxygen minima and lateral fluxes in this region.

Plain Language Summary

The ocean region located along the south-western African coast, known as the Benguela Upwelling System, hosts an important fishery for human sustainment. We studied variability and drivers of recurrent low oxygen events that characterise this region and that can impact the local ecosystem and affect fisheries yields. We used four months of data collected ∼100 km from the coast, spanning from the ocean surface to 1000 m depth. We found that oxygen concentrations damaging for fish occurred mostly between ∼70m and 550m of depth, for about 30% of the time. Such low oxygen concentrations lasted for about one week each time, and were brought into the Benguela region by deep fluxes of low-oxygen water from the northern Angola latitudes. Rotating flow structures of a typical diameter of between 20 and 200 km, known as ocean eddies, were found to strongly impact oxygen concentrations in the region by either transporting very low oxygen water or by stirring and mixing water masses with different oxygen levels. The variability in oxygen concentrations found by this study likely affects the local ecosystem and further studies will be needed to better understand its seasonality and future trends in the context of climate change.

1 Introduction

Ocean oxygen (O_2) concentrations influence the distribution and functioning of marine life and are determined by a combination of physical and biological mechanisms (Garçon et al., 2019; Fennel & Testa, 2019; Pitcher et al., 2021). The near-surface ocean is generally well oxygenated: there, oxygen levels are mostly regulated by a combination of temperature-dependent and fast air-sea exchange fluxes balancing oxygen super- or undersaturation and biological activity, especially primary production in the euphotic layer, which adds oxygen via photosynthesis (Sarmiento & Gruber, 2006). Below the euphotic layer, advection and mixing (both horizontal and vertical) and biological activity in the form of remineralisation and respiration dominate the O_2 budget. While respiration always acts as a sink for O_2, contributing to the formation of deep oxygen-minima, physical fluxes can either increase or decrease O_2 concentrations depending on their source region (Wyrtki, 1962). Ocean ventilation, i.e., the deep injection of well-oxygenated surface waters via mixing or advection, acts to replenish the deep oxygen budget. Lateral fluxes, upwelling

and small scale variability connected to meso- and submesoscale eddies and fronts further modulate the oxygen field by influencing a variety of biological processes, which in turn modify O_2 concentrations (Frenger et al., 2018; Löscher et al., 2016; Brandt et al., 2015).

Variability in ocean oxygen concentrations has been extensively studied in the past decades, especially in relation to the expansion of the oxygen minimum zones (OMZs) driven by anthropogenic forcing (Pitcher et al., 2021; Schmidtko et al., 2017; Ito et al., 2017). Spatio-temporal changes in oxygen concentration can constitute significant stressors for marine ecosystems and can have potentially lethal effects on important fisheries (Grantham et al., 2004; Ohde & Dadou, 2018). Most marine heterotrophs, including higher animals such as fish, die when exposed to oxygen concentrations below a certain critical threshold, which varies significantly among species (Keeling et al., 2010; Vaquer-Sunyer & Duarte, 2008). Even intermittent occurrences of such lethal oxygen levels can result in behavioural changes due to the need to frequently escape such conditions, and can result in declining growth rates in juvenile fish (Eby et al., 2005). The median lethal time in low-oxygen conditions also varies greatly from species to species, and ranges from several months to as little as half an hour (Vaquer-Sunyer & Duarte, 2008). As a consequence, low oxygen levels effectively constitute a biogeochemical boundary for most marine species and can strongly affect the ecosystem composition and predator/prey interactions (Gibson & Atkinson, 2003).

Among the regions most affected by deoxygenation, eastern boundary upwelling systems (EBUS) are extremely significant (Garçon et al., 2019; Löscher et al., 2016; Karstensen et al., 2008), as they bound some of the ocean's major OMZs while also hosting high levels of coastal productivity that supports some of the most important fisheries for human sustainment (Carr & Kearns, 2003; Mackas et al., 2006; Kainge et al., 2020). The Benguela Upwelling System (BenUS), one of four major EBUS, is located along the south-western African coast, at the eastern edge of the South Atlantic gyre, between roughly 18°S and 34°S (Chavez & Messié, 2009; Hutchings et al., 2009; Sowman & Cardoso, 2010). As with all EBUS, the BenUS is characterised by high levels of mesoscale and submesoscale activity in the form of surface and subsurface intensified eddies, filaments and fronts, which have an important role in modulating marine oxygen levels via a variety of biophysical interactions (Mohrholz et al., 2014; Frenger et al., 2018; Thomsen, Kanzow, Colas, et al., 2016; McGillicuddy, 2016).

At its northern edge, the BenUS is bounded by the Angola-Benguela frontal zone (ABFZ), which separates the system from the equatorial region of Angola and is located roughly between 15°S and 18°S (Veitch et al., 2006). The ABFZ is characterised by significant meridional gradients of physical and biogeochemical tracers, including temperature, salinity and oxygen, which reflect the different properties of the water masses located at its northern and southern edges (Veitch et al., 2006; Kostianoy & Lutjeharms, 1999; Bartholomae & van der Plas, 2007). North of the ABFZ, the equatorial cyclonic circulation of Angola is dominated by the warm, saline and oxygen-depleted South Atlantic central water (SACW) and hosts the most intense OMZ of the Atlantic ocean (Bartholomae & van der Plas, 2007; Karstensen et al., 2008; Stramma et al., 2008). South of the ABFZ, the BenUS is crossed by the along-shore northward-flowing Benguela Current, which carries relatively colder, fresher and oxygenated eastern South Atlantic central water (ESACW), a blend of equatorial SACW and Indian central water (ICW) transported into the South Atlantic by the Agulhas Current (Siegfried et al., 2019; Mohrholz et al., 2008). At the ABFZ, the northward-flowing Benguela Current and the southward-flowing Angola Current converge along the coast and are deflected westward towards the open ocean, with a slight northward tilt (Figure 1b). Variability in the temperature and salinity of the region surrounding the ABFZ and in the latitudinal location of the front can be determined by interannual fluctuations known as Benguela Niños/Niñas as well as seasonal and in-

traseasonal shifts in the the atmospheric wind pattern (Veitch et al., 2006; Kostianoy & Lutjeharms, 1999; Diakhaté et al., 2016).

Along-shore fluxes recurrently cross the ABFZ (Boyer et al., 2000; John et al., 2000). At the surface, the Angola Current can intrude into the northern BenUS along the shelf in the shape of a tongue of surface warm water, especially in December-March (Muller et al., 2014; Bartholomae & van der Plas, 2007; Shannon et al., 1987); at depth, a subsurface flow of Angola water extends far into the Benguela region with maximum intensity in January-February (Mohrholz et al., 2008; Rouault, 2012; Stramma & England, 1999). Such cross-frontal fluxes happen as a result of both wave propagation and local wind forcing (Tchipalanga et al., 2018). Equatorially-forced coastal trapped waves that flow along the continental shelf transporting Angola water southward constitute a mode of coupling between the equatorial region and the BenUS and can transfer variability ranging from the sub-seasonal to interannual scales (Illig & Bachèlery, 2019; Bachèlery et al., 2020; Kopte et al., 2017). Coastal-trapped waves forced by local winds can further modulate the shelf flow on the faster scales of a few days to weeks, either enhancing or stopping the propagation of the poleward shelf current (Junker et al., 2019). Further connection between the tropical circulation and northern Benguela is provided by the southeastward flow of the equatorial currents (Siegfried et al., 2019). The along-shore advection of low-oxygen anomalies from the north has been shown to be the primary driver of oxygen variability on the shelf of the northern BenUS (Monteiro et al., 2006). Local remineralisation can further exacerbate these conditions (Ohde & Dadou, 2018).

So far, most studies have focused on the oxygen variability on the BenUS shelf, with only a limited analysis of the impact on the adjacent open waters off the northern Benguela shelf. Further, observations focusing on the short-term fluctuations in the oxygen concentration and the impact of mesoscale variability in such a dynamic region are still lacking. Here we use four months of high-resolution glider data collected 100 km from the BenUS coast to investigate the temporal variability of oxygen concentrations in the open waters off the shelf of the northern BenUS, focusing on significant fluctuations observed in the upper mesopelagic (100 m - 500 m) and their relation to the dominance of SACW and ESACW. Further, we discuss the duration, intensity and depth distribution of the hypoxic events, and present two distinct examples of how meso- and submesoscale activity shapes oxygen concentrations in our data. Last, we put our results in the context of previous research in order to identify the physical drivers of the observed variability and present our conclusions.

2 Methods

2.1 Glider data

One Slocum glider was deployed on 14 February 2018 at 11.2 °E, 19.3 °S in the region of the northern BenUS (Figure 1a) by the European Research Council project Gauging ocean Organic Carbon fluxes using Autonomous Robotic Technologies (GOCART), in conjunction with the Controls over Ocean Mesopelagic Interior Carbon Storage (COMICS) programme (Sanders et al., 2016). The glider was deployed 3 months ahead of the COMICS cruise (which occurred in May 2018) in order to characterise the water column dynamics and temporal variability in this region. The glider transited north for 3 days from its deployment location to the sampling site BN0 [10.80 °E, 18.25 °S], where it profiled to 1000m depth from 17 February 2018 until 26 March 2018. On 27 March 2018, the glider moved slightly north-east to measurement point BN, centered around [10.95 °E, 18.05 °S], where it sampled until 19 June 2018, when it was recovered. The two measurement spots are located at about 120 km (BN0) and 95 km (BN) from the south-western African coast and are separated from each other by roughly 27 km. Both locations are off the continental shelf, north of the Walvis Ridge, in a region with maximum bathymetry of about 3000 m.

At each sampling location, the glider followed a triangular path of $\sim$ 12 km per side which took between 2 days in February-May to 5 days in June to complete. The glider completed profiles to 1000 m depth, sampling with a vertical resolution of $\sim$ 20 cm, emerging 5 to 6 times per day and sampling primarily on the upward dive. A few sets of consecutive downcast-upcast were collected throughout the deployment to allow the determination of oxygen sensor time response. The glider was fitted with a standard Slocum Glider Payload CTD (pumped) from Seabird (SN 9109), measuring Temperature, Conductivity and Depth, with an Aanderaa optode, model 4831 (SN286), measuring dissolved oxygen, and a Seabird WetLABS ECO triplet sensor, measuring optical backscattering at 700 nm. Depth-averaged currents (DAC) were estimated for each full 1000 m downward and upward dive from the difference between the glider's observed surfacing location and that predicted by the glider's onboard dead reckoning or flight model (SLOCUM manual, 2017; Merckelbach et al., 2010). For each glider surfacing, glider surface currents were also estimated via linear regression of GPS location with respect to time. Median timescale of surface current estimates, defined as the interval between first and last GPS fix was 21 min with 95% between 10 and 48 min. It is worth noticing that glider estimates of surface currents may be subject to a wind influence as the glider tail may acts temporarily as a sail in strong wind conditions.

In the present analysis, conservative temperature (T_c, from here on: temperature), absolute salinity (S_a, from here on: salinity), potential density (σ_θ) and dissolved oxygen (O_2) glider data are used in the form of binned medians, with each bin representing an interval of 6 hours in time (usually 1-2 profiles) and 2 m in depth. Glider surface and DAC velocities were averaged daily. Backscatter data ($b_{bp}700$) are averaged on coarse bins spanning one day in time and 10 m in depth. Please, note that in this manuscript backscatter data is used only qualitatively to strengthen some of our hypothesis and is only presented in the Supplement. As the glider measurements were collected during 2018, we will implicitly refer to this year throughout the rest of the manuscript.

Glider temperature and salinity values were initially calculated using factory calibrations. Next, lag-corrected oxygen data were calculated by applying the following steps: (1) calculate sensor time response, determined by shifting the reported oxygen in time and find the time lag that corresponds to the minimum total discrepancy between consecutive profiles (up-down and down-up) of oxygen (50 s for this glider); (2) apply time lag correction to raw sensor output "calphase"; (3) calculate oxygen concentration using the coefficients from factory multi-point calibration; (4) apply temperature, salinity and pressure correction following manufacturer recommendations. Finally, shipboard CTD profiles collected during COMICS cruise DY090 were used to validate glider temperature and salinity measurements and adjust glider oxygen measurements, in a two-step process. First, salinity and dissolved oxygen sensors mounted on the ship's CTD package were calibrated using linear regressions against 113 bottle salinity measurements (using an Autosal 8400B) and 261 bottle oxygen measurements (using the Winkler titration method). Second, all shipboard and glider sensor profiles were binned at 5 m depth intervals and "ship-glider matchups" were selected for glider calibration, defined as binned profiles within 5 km and 12 h of each other. These matchups were strongly correlated (linear regression $r^2 \geq 0.95$). Paired binned data from all matchups (n=18 for temperature, n = 17 for salinity, and n= 16 for oxygen, where n is the number of CTD casts) were combined to calculate a single linear regression of ship data vs. glider data. Glider temperature and salinity data matched ship data within uncertainty of the regressions and were therefore not corrected. Glider oxygen data were corrected using the regression slope (1.03) and offset (+1.72 µmol kg^{-1}) found in the calibration exercise (see Supplement Figure S14). Gliders measured optical backscattering at 700 nm using Seabird ECO triplet sensors. Factory calibrations were applied to raw data to yield estimates of the total volume scattering function β(700 nm, 124°). The volume scattering function of seawater was estimated following Hu et al. (2019) and subtracted to yield the particulate volume scattering function β_p(700 nm, 124°) and then converted to the partic-

ulate backscattering coefficient b_{bp}(700 nm) via b_{bp}(700 nm) = β_p(700 nm, 124°) $2\pi\chi$, where $\chi = 1.077$ (Sullivan et al., 2013).

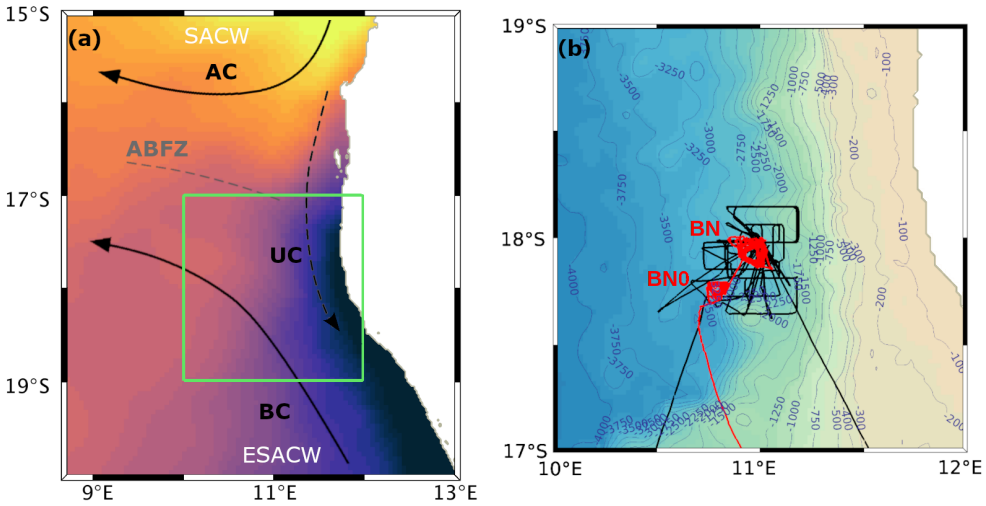

Figure 1. (a) Schematic representation of the regional system of currents and of the water masses carried by them, as described by the literature presented in the Introduction: Angola current (AC), Benguela current (BC), Angola-Benguela frontal zone (ABFZ), cross-front undercurrent (UC), South Atlantic Central Water (SACW), Eastern South Atlantic Central Water (ESACW). This scheme is a simplification of the regional current schemes by Rouault et al. (2007), Hardman-Mountford et al. (2003) and Siegfried et al. (2019). This is only a conceptual scheme which does not intend to be an exact representation of the system of currents nor of the location of their maxima. The green square indicates the perimeter of subplot (b). Colour shading: SST from L4 AVHRR REP Ostia (Good et al., 2020) averaged across the glider measurement period. (b) Glider (red) and ship (black) tracks on the regional GEBCO (2019) topography [m]. Labels indicate the spots BN0 and BN in which the glider collected data.

2.2 Water mass identification

The glider measurements were collected at the northern boundary of the BenUS (Figure 1a), in the proximity of the ABFZ. We identify the two central water masses in the glider data by converting the SACW and ESACW water mass boundary values of Mohrholz et al. (2008); Poole and Tomczak (1999); Flohr et al. (2014) for in-situ temperature T_i and practical salinity S_p into units of absolute salinity (S_a) and conservative temperature (T_c) using the TEOS-10 Gibbs Seawater (GSW) Oceanographic Toolbox (McDougall & Barker, 2011). We acknowledge that the conversion from T_i and S_p to T_c and S_a is non-linear. However, we used these points to qualitatively assess the presence of the two water masses in the glider data by plotting the line that connects the extreme values of T_c and S_a for each water mass, which is sufficient for our purposes. Please refer to Supplement Table S1 for the details of the conversion and the adopted values of T_c and S_a.

We also used World Ocean Atlas 2018 (WOA18) data (NOAA data set, 2018; Garcia et al., 2019) to compare the glider absolute salinity and oxygen data to the long-term mean regional profiles. Salinity from WOA18 was transformed into units of absolute salinity (S_a) using the tools described in the previous paragraph. Mean profiles were calculated using the 1° gridded product for the offshore Angola waters north of the glider in

the range [9°E,11°E] x [15°S,17°S] and for the offshore Benguela waters south of the glider in the range [10°E,12°E] x [21°S,23°S]. Mean WOA18 profiles were calculated from climatological (1955-2017) monthly means from February to June. Given the strong variability and sharp lateral gradients that characterize the measurement region, this analysis provides more information than comparing the glider data with sporadic measurements or coarse resolution products around the glider location.

2.3 Glider data analysis: tracer anomalies and stratification

In order to highlight the time variability in the tracer concentrations in the glider data, we calculated tracer anomalies from their mean vertical profiles over the entire period of sampling. Although this does not remove the seasonal trends in the glider data, we found this choice to be more appropriate than the use of a running mean, due to the limited temporal extent of the measurements and sharp horizontal and vertical gradients found by the glider. Further, this choice allows us to explore both the short scale and the lower frequency variability in the tracers. We therefore take into account both the role of small scale variability and the role of seasonality in the discussion of the tracer anomalies.

The mixed layer depth (MLD) was calculated according to a temperature criterion, as the deepest depth at which $T = T_{10m} \pm 0.8°\mathrm{C}$ (Kara et al., 2003). As a measure of water column stability, we calculated the Brunt-Väisälä frequency, defined as:

$$N^2 = -\frac{g}{\rho_0} \cdot \frac{\partial \sigma_\theta}{\partial z} \tag{1}$$

where $\frac{\partial \sigma_\theta}{\partial z}$ is the derivative of potential density with respect to depth, g is gravitational acceleration and $\rho_0 = 1026$ kg m^{-3} is the mean reference density of seawater, corresponding to our average density in the most dynamic first 400 m depth.

2.4 Regional setting during the measurement campaign

We used several data products to identify the large-scale physical and biogeochemical context in which the glider measurements were taken. The evolution of currents, sea surface temperature (SST) and chlorophyll (CHL) concentration were evaluated from daily-mean satellite data. We ran the algorithm by Faghmous et al. (2015) on each time step of the AVISO sea surface height (SSH) field (CMEMS, 2022) to identify the eddies, each one defined as the area within the outermost closed SSH contour containing a single SSH minimum (cyclonic eddy) or maximum (anticyclonic eddy). SST was taken from the L4 AVHRR REP Ostia dataset (Good et al., 2020), consisting of gap-free maps combining high-resolution data in cloud free conditions (1/20 ° resolution) and lower resolution images (1/4 ° resolution). Daily mean surface CHL was taken from the L3 GlobColour dataset (CMEMS, 2020) at a spatial resolution of 4 km.

We used the in-situ glider estimates of near surface currents and DAC, as well as ship, satellite and reanalysis products to evaluate the near-surface flow at the glider position. Ship measurements of near-surface velocities (30 m depth) were collected using a shipboard acoustic doppler current profiler (Teledyne RDI ADCP Ocean Surveyor, 75 KHz) at measurement point BN from 02 June 2018 until the end of the measurement campaign on 19 June 2018 (Figure 1a), and they were averaged daily for the present analysis. Additional gridded products were co-located with the glider using a nearest-neighbor routine that calculates a weighted average of the velocities at the closest four grid points from the glider on each day. We used daily mean AVISO and GlobCurrent satellite data at 1/4 ° resolution (CMEMS, 2022; Rio et al., 2014). Both datasets are based on the same SSH-derived geostrophic currents, however GlobCurrent uses additional modeled Ekman transport to better capture the nearshore wind-driven dynamics. Note that the AVISO product often underestimates the westward wind-driven currents, resulting at times in

excessive eastward flow, for example in early April when the AVISO surface flow results exceeds all the other products; GlobCurrent, however, at times seems to overestimate the westward (off-shore) transport in disagreement with the observed SST and CHL fields, especially in late April. A comparison of the two fields is provided in the Supplement (Figure S3). On cloud-free days, surface currents at 30 km resolution were estimated by spatially correlating consecutive images of L2 surface CHL data from MODIS Aqua, MODIS Terra, and VIIRS at 1 km resolution (NASA-OBPG, 2018a, 2018b, 2018c) via the maximum cross correlation method (Crocker et al., 2007; Liu et al., 2017); daily fields were calculated as the median of the available surface velocity data for each day. We also used daily mean surface velocities from the GLORYS12v1 reanalysis product (Drévillon et al., 2018; Fernandez & Lellouche, 2018) based on the Operational Mercator global ocean analysis and forecast system which uses the physical model NEMO forced with ERA5 reanalysis data (Madec & Team, n.d.; Hersbach et al., 2020) on a 8km-resolution grid. A list of the employed datasets is provided in Supplement's Table S2.

2.5 Upwelling indexes

We calculated the wind-driven upwelling components using daily mean wind stress from ERA5 reanalysis (Hersbach et al., 2020) at 1/4° resolution. To calculate the coastal upwelling index (U_i), we rotated the wind stress (τ) components in the alongshore (AS) direction, averaged it in the first 100 km from the coast, and then used:

$$U_i = \frac{\tau_{AS}}{f\rho} \tag{2}$$

where f is the latitude-dependent Coriolis parameter and ρ is the density of seawater (same as Subsection 2.3). U_i was averaged in the latitude range [17°S,19°S], in the proximity of the glider. To calculate Ekman pumping, we calculated the curl of the wind stress and derived the Ekman pumping velocity w_{EKP}:

$$w_{EKP} = \frac{\nabla \times \vec{\tau}}{f\rho} \tag{3}$$

from which we obtained the pumping velocity at the glider position w_{gl} by selecting the grid point at [11°E,18°S]. To obtain the nearshore Ekman pumping index W_i we calculated the volumetric transport via an area integral of w_{EKP} in first 100 km from the coast in the range [17°S,19°S] and divided this by the coastline length in the same range. This way both upwelling indexes are in units of volumetric water transport per meter of coastline ($m^2\ s^{-1}$). Following Messié et al. (2009), to calculate W_i we set negative values w_{EKP} to zero before integration, to reflect the asymmetry in the transport of nutrients.

2.6 Low oxygen thresholds

Throughout the manuscript, we study low oxygen events during which concentrations fall below a set of three thresholds: $O_2 < 120$ µmol kg^{-1}; $O_2 < 60$ µmol kg^{-1}, here defined as hypoxia; and finally $O_2 < 30$ µmol kg^{-1}, here defined as severe hypoxia. These thresholds are intended to highlight a set of critical oxygen conditions for different marine organisms. Our loosest threshold of 120 µmol kg^{-1} is used to represent the mean sub-lethal oxygen threshold for fish (triggering behavioral and metabolic changes) as well as the lethal threshold for sensitive crustacean and fish larvae (Vaquer-Sunyer & Duarte, 2008; Ekau et al., 2010). Our hypoxic threshold (60 µmol kg^{-1}) closely represents the mean lethal oxygen concentration calculated across a wide range of marine species, and is commonly adopted for studies of the impact of low oxygen events on fisheries (Zhang et al., 2010; Vaquer-Sunyer & Duarte, 2008; Gilly et al., 2013). Severe hypoxia ($O_2 <$ 30 µmol kg^{-1}) indicates critical conditions for some low oxygen-resistant organisms such as gelatinous plankton, squids and copepods (Ekau et al., 2010). When evaluating the depth range affected by low oxygen anomalies for each threshold, we exclude regions in which the anomalies are observed for less than 1% of the deployment period.

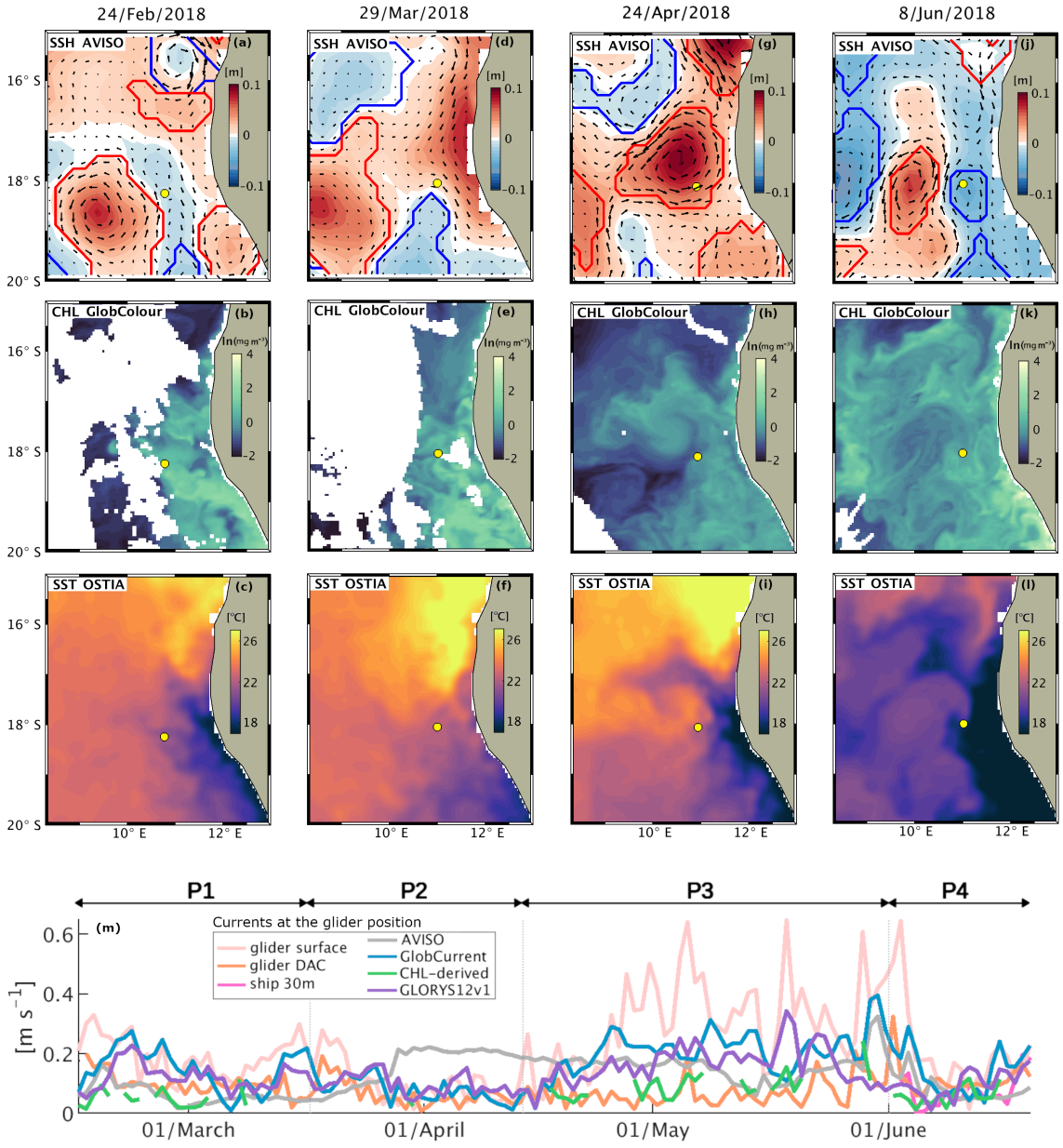

Figure 2. Regional setting from satellite data on 24/February (a-c), 29/March (d-f), 24/April (g-i), 08/June (j-l). First row: SSH [m] with geostrophic velocities from AVISO. Second row: surface CHL [ln(mg m^{-3})] concentration from GlobColour. Third row: SST [°C] from L4 AVHRR-Ostia. Line contours on SSH indicate the identified cyclonic (blue) and anticyclonic (red) eddies. White areas in CHL images indicate missing data due to cloud cover. The mean daily glider position is indicated by a yellow dot. (m) Horizontal velocities (absolute) at the glider position from satellite data (AVISO, GlobCurrent), satellite chlorophyll derived data (CHL-derived), model reanalysis data (GLORYS12v1), glider data both at the surface (glider SURF) and depth-averaged (glider DAC), and ship data for velocities at 30 m depth. The duration of phases P1 to P4 is indicated by the horizontal arrows above subplot (m), each one also corresponding to the satellite images in the column above it.

3 Results

3.1 Regional setting

The glider data were collected during February-June 2018, i.e., during the period spanning from the low upwelling season to the early phase of the winter upwelling season of the northern Benguela (Hutchings et al., 2009). SST anomalies for 2018 indicate neutral Benguela Niño conditions (Imbol Koungue et al., 2021). Satellite images and horizontal velocity products (Figure 2) show a succession of very different conditions in the region surrounding the glider. We identify four periods (P1-P4), each one characterised by a specific type of dynamics. Phase 1 (P1: 14/February - 16/March) is characterised by moderate currents at the glider position, by a cold water signature along the BenUS coast and by a complex regional pattern of high-CHL filaments; the glider is located north-east of a large and persistent anticyclone and surface satellite images suggest that the glider is hit from south-east by cold and high CHL coastal water. Phase 2 (P2: 17/March - 13/April) is characterised by minimum surface flow at the glider position and by a tropical warm water intrusion along the Benguela shelf visible as a narrow low-CHL and warm SST anomaly reaching down to 19 °S, which temporarily reverses the cross-shore SST gradient. Phase 3 (P3: 14/April - 31/May) is characterised by the formation (late April), intensification (early May) and drifting/dissipation (late May) of a large frontal anticyclone at the ABFZ (see also Supplement Figures S1,S2). During this period horizontal currents at the glider position intensify, peaking in early May when the glider is located at the outer edge of the anticyclone in a region characterised by sharp gradients of chlorophyll, while coastal upwelling pulses and large fluctuations in the zonal and meridional currents indicate strong winds and turbulence. Phase 4 (P4: 01/June - 19/June) is characterised by blooming conditions and a cooling of the SST likely due to a combination of pulses of upwelling in early June and the transition towards Austral winter. The glider is embedded in the cold-water front originating at the Benguela shelf and including a weak cyclonic eddy.

3.2 Water column properties from the 2D glider transects

The glider data show clear fluctuations in the tracer distributions at all depths to at least 500 m depth (Figure 3). The water column was rather stratified, with a mean MLD of 35 m, rarely exceeding 50 m. The distinct timescales of variability of near-surface and deeper water properties suggests some degree of decoupling between these layers and a shift in the dominant drivers of tracer fluctuations, with an abundance of deep water T_c and S_a anomalies that are not reflected by the surface fields.

At depths of 50 - 500 m, water properties are very dynamic, characterised by alternating positive and negative anomalies in temperature and salinity. In this range of depths, in fact, temperature and salinity are characterised by a qualitatively similar pattern of positive and negative anomalies that alternate each other, lasting for periods that range between a few days and a few weeks. Some of the short timescale variability in the transects, persisting throughout the entire data series and generating sub-weekly oscillations, is likely associated with the lateral movement of the glider around the sampling triangle, and is therefore a signature of spatial, not temporal, gradients. Below 500 m depth, tracer oscillations are more moderate and persist for longer periods than in the upper layers, suggesting a further shift of the variability drivers from the more dynamic upper mesopelagic region (see also Supplement Figures S5,S6 for the full depth transects).

The temperature and salinity diagram of the sampled water masses shows that the known T_c-S_a curves of SACW and ESACW constitute the extreme boundaries of the central water masses measured by the glider (Figure 4a). As expected given the known characteristics of the two water masses, points located on the SACW line are characterised by very low oxygen concentrations, often falling below 60 µmol kg^{-1}, while those located in correspondence with ESACW are characterised by oxygen concentrations of at least

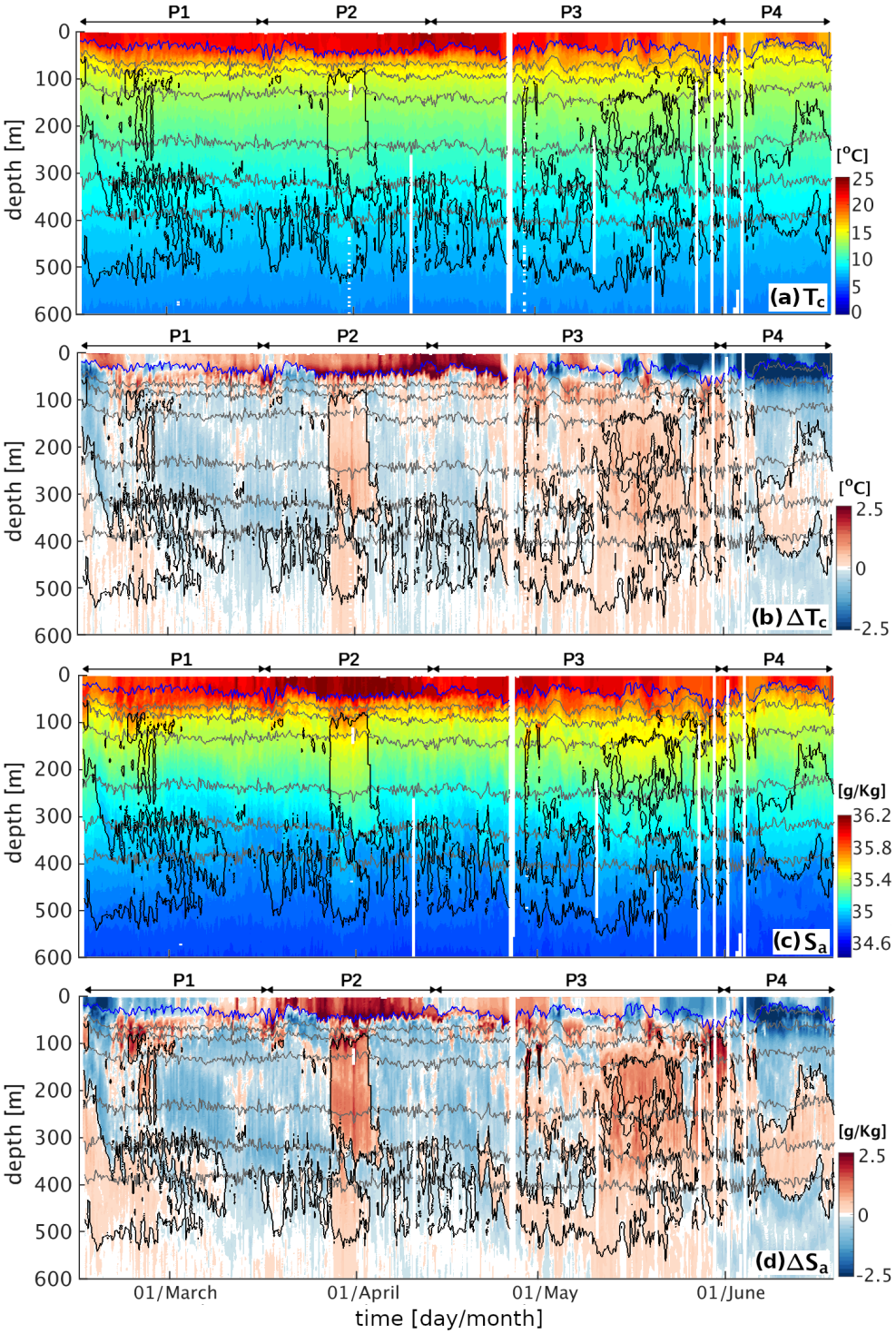

Figure 3. Glider transects up to 600 m depth: (a) conservative temperature, (b) conservative temperature anomaly, c) absolute salinity, d)absolute salinity anomaly. Gray lines: isopycnals for 26, 26.25, 26.5, 26.75, 26.9, 27 [kg m^{-3}]. Black lines: outer boundary of hypoxic regions (O_2 = 60 µmol kg^{-1}). Blue line: MLD [m]. Full profiles to 1000 m depth are available in the Supplement (Figures S5,S6).

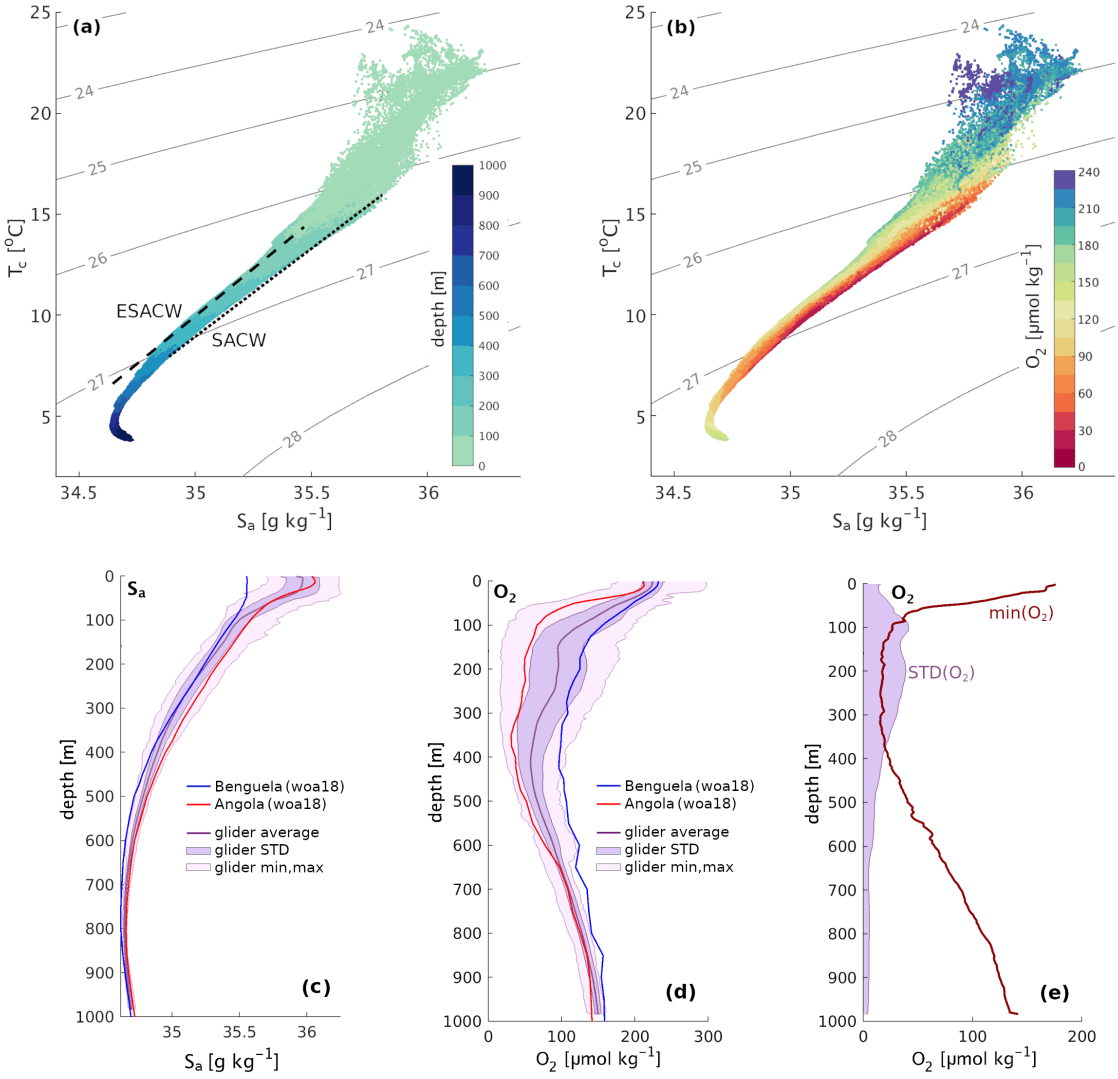

Figure 4. (a-b) Conservative temperature (T_c) and absolute salinity (S_a) diagram of the binned glider data, with density isolines in gray [kg m^{-3}] and dots coloured according to: (a) depth, (b) oxygen concentration. (a) The characteristic T_c-S_a trends of SACW and ESACW are highlighted respectively by a dotted and a dashed black line. (c,d) Mean profile, standard deviation range and minimum-maximum range for (c) absolute salinity and (d) oxygen from the glider data (purple line and shadings) compared to climatological mean profiles across the period February-June for the offshore Angola (red lines) and Benguela (blue lines) from World Ocean Atlas 2018 (see Methods). (e) Depth profile of the standard deviation and minimum of oxygen from glider data.

100 µmol kg^{-1} (Figure 4b). Such T_c-S_a diagrams and the observed fluctuations in physical properties point towards a co-presence of water from the northern Angola and from the southern latitudes of the BenUS at the glider position, with the two water masses alternating each other between 100 m and 500 m depth. This result is further emphasised by a comparison of the vertical S_a and O_2 profiles at the glider position with the climatological mean vertical profiles of the offshore Angola and Benguela waters (Figure 4c,d), showing a remarkable correspondence between the climatological profiles and

the range of values measured by the glider. Interestingly, a large number of points fall between the SACW and ESACW lines in both our T_c-S_a diagrams and in the vertical profile plots, therefore suggesting that part of the two water masses mix with each other in the region of sampling.

3.3 Oxygen variability and its relation to water properties

Glider data show that oxygen concentrations drop significantly across the first 100 m depth (Figure 5). The MLD is characterised by values above 200 µmol kg^{-1} and constitutes the only near-surface range where oxygen consistently exceeds the sublethal threshold of 120 µmol kg^{-1}. The mean oxygen concentration drops below this threshold at 110 m depth and oxygen concentrations exceeding sublethal levels are observed sporadically at larger depths. At around 100 m depth, minimum O_2 values also drop quickly to just 25 µmol kg^{-1} (Figure 4e).

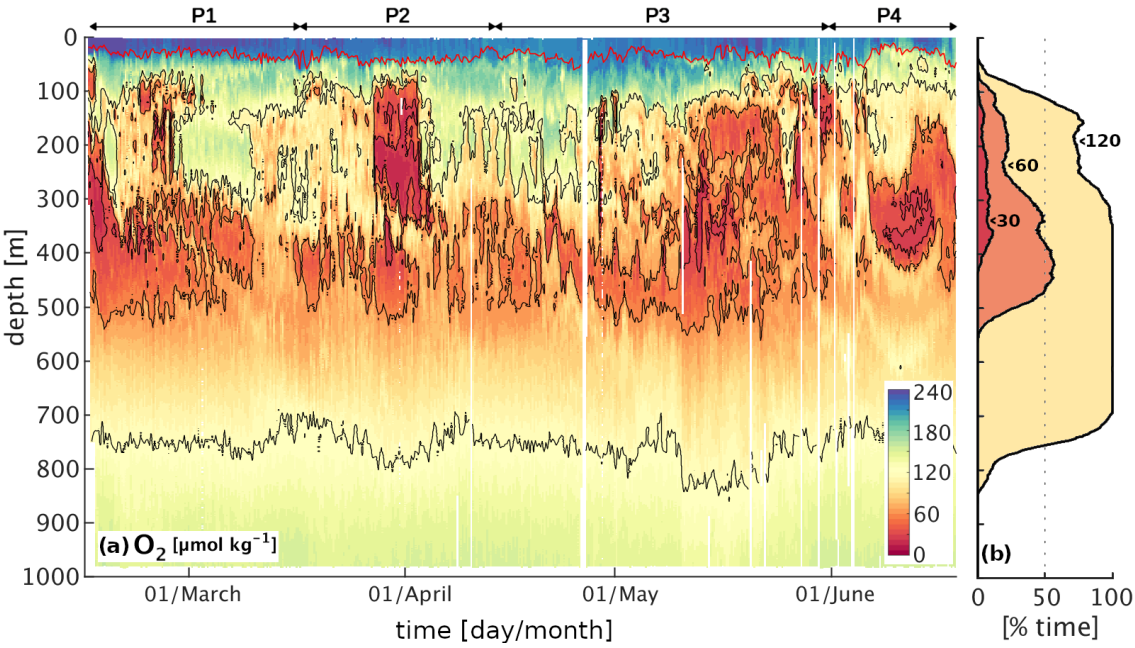

Figure 5. (a) Oxygen transect from glider data with black isolines of concentration at 30 µmol kg^{-1}, 60 µmol kg^{-1}, 120 µmol kg^{-1} and mixed layer depth in red; (b) percent of total time in which oxygen is below 30 µmol kg^{-1} (red), 60 µmol kg^{-1} (orange) and 120 µmol kg^{-1} (yellow) as a function of depth.

The temporal variability in the oxygen concentration increases significantly below the MLD (Figure 5a), where it closely follows the pattern of ΔT_c and ΔS_a. This shift is due, on the one hand, to the lack of air-sea exchange fluxes and a limited impact of biological production below the near-surface layer, and, on the other hand, to the significant role of the deep lateral influx of northern warm/saline/oxygen-depleted SACW and southern cold/fresh/oxygenated ESACW, as highlighted by the association of positive temperature and salinity anomalies with negative oxygen anomalies. This interpretation is further supported by a comparison in time between the sampled salinity and oxygen profiles and the climatological mean salinity and oxygen properties of the waters found north of the glider (offshore Angola) and south of the glider (offshore Benguela), showing a remarkable match between salinity and oxygen properties with the two water masses (Figure 6). As a result, hypoxic events in the upper mesopelagic at the glider

position can be attributed to the dominance of saline and de-oxygenated water from the northern latitudes, while higher oxygen levels are carried into the region by fresher central waters from southern Benguela latitudes.

Although local remineralisation likely further modulates the O_2 profile at the glider position, our analysis highlights that the dominant drivers of the sub-monthly oxygen variability within 100-500 m depth are physical, resulting in weekly to bi-weekly hypoxic events associated to shifts in temperature and salinity. Importantly, this high variability implies that sporadic observations are unlikely to capture the average oxygen profile in this region, likely sampling temporary fluctuations around the mean. Further, a decoupling between the observed variability of the near-surface and of the deeper water properties suggests that the signature of these alternating fluxes of water masses may not always be detectable from the surface. Indeed, evidence of a southward transport in the satellite data emerges clearly only on the shelf during P2 and at the glider position in relation to the anticyclonic recirculation of tropical water across the front during P3 (Figure 2).

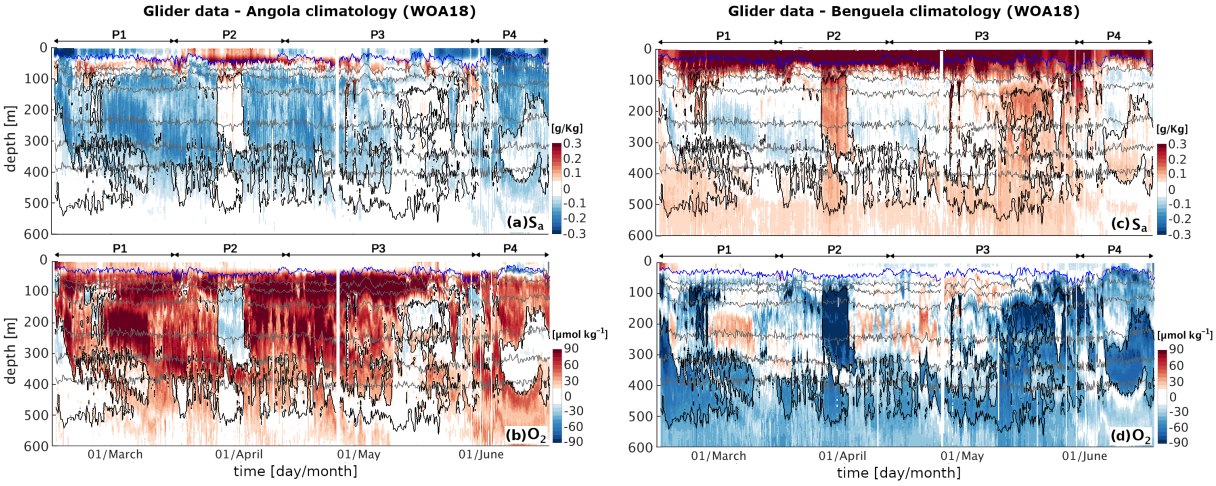

Figure 6. Difference between the glider data transects and the climatological mean profiles across the period February-June for the offshore Angola (a,b) and offshore Benguela (c,d) water properties (see Methods). (a,c) Absolute salinity S_a difference and (b,d) oxygen O_2 concentration difference. White shading covers the range [-0.05, 0.05] kg m^{-3} for S_a, and [-15, 15] µmol O_2 m^{-3} for O_2. Gray lines: isopycnals for 26, 26.25, 26.5, 26.75, 26.9, 27 [kg m^{-3}]. Black lines: outer boundary of hypoxic regions (O_2 = 60 µmol kg^{-1}). Blue line: MLD [m]. Full profiles up to 1000 m depth are available in the Supplement (Figures S8,S9).

3.4 Oxygen variability: intermittency of hypoxia

As a consequence of the alternating dominance of SACW and ESACW, both hypoxia and severe hypoxia observed in the upper mesopelagic are intermittent throughout the entire measurement period (Figure 7). Hypoxic events (O_2 < 60 µmol kg^{-1}) are confined between ∼70 m and ∼550 m depth, where they occur for an average of ∼30 % of the deployment, increasing to ∼50% within the sub-range of 300 m and 450 m depth (Figure 5b). Severe hypoxic events, in contrast, are shallower and more confined vertically, being observed only between ∼110 m and ∼420 m and occurring on average for ∼6 % of the total measurement time. Severe hypoxic events ranged in timescale from <1 day to ∼1 week, with the largest single event occurring in the beginning of April (P2),

when severe hypoxia was observed just below 100 m depth (Figure 5). More sporadic severe hypoxia is also detected at deeper depths by the glider during the early (P1) and late measurement period (P3-P4), the latter following some bursts of coastal upwelling (see also Supplement Figure S2).

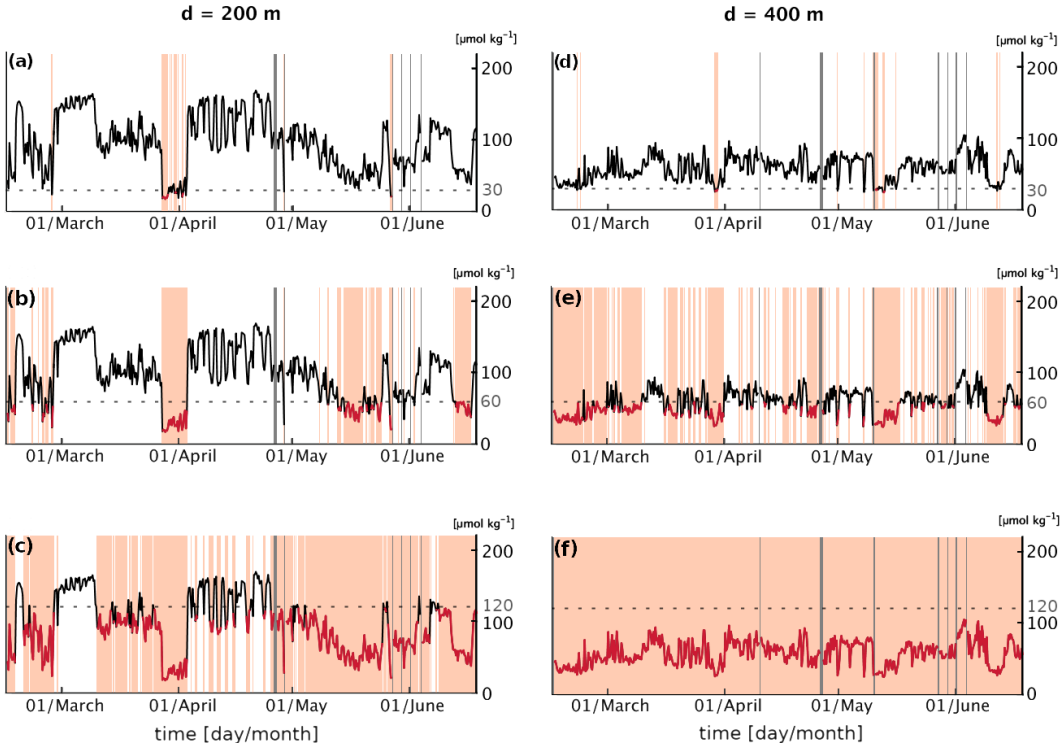

Figure 7. Time variability and duration of the low oxygen events at two different depths of reference, one per column for the three oxygen thresholds evaluated: (a-c) 200 m, ∼22 % probability of occurrence of hypoxia; (d-f) 400 m, ∼54 % probability of occurrence of hypoxia. Orange shading highlights when oxygen falls below a certain threshold, indicated by the horizontal dashed gray line: (a),(d) 30 µmol kg^{-1}; (b),(e) 60 µmol kg^{-1}; (c),(f) 120 µmol kg^{-1}. Gray shading indicates missing data.

In order to correctly interpret the results we must keep in mind the spatio-temporal nature of the observed fluctuations. As the glider was repeatedly visiting the same locations while moving along a triangular path of 12 km of side, the observed variability is due to a combination of temporal changes in the dominant water mass and spatial gradients, the latter generating oscillations with a period of 2 days during February-May and 5 days in June, when the glider slowed down. Sub-weekly fluctuations in O_2 concentration and salinity (Figure 5) therefore indicate that the glider was moving across sharp gradients of oxygen, highlighting spatial patchiness in O_2 and sharp gradients at the region of sampling. Weekly and persistent fluctuations, on the other hand, are associated with larger scale shifts in the pattern of water masses at the glider position and therefore on significant changes in the pattern of currents intersecting the region of sampling.

Our data shows that, in the depth range where hypoxia is most persistent (300 m to 450 m depth) the glider-derived mean oxygen and salinity profiles are closer to the climatological profiles of the Angola latitudes (Figure 4c,d), suggesting that the presence of subsurface SACW is more persistent at these depths. On the contrary, in the shal-

lower depth range between 100 m and 300 m, where we can identify weekly and bi-weekly pulses of hypoxia and intense salinity anomalies, the glider oxygen and salinity profiles show a large standard deviation and fall just between the Angola and Benguela profiles (Figure 4), indicating a higher degree of temporal variability in the influence of SACW and ESACW. Interestingly, a few of the low oxygen anomalies, such as the early-April severe hypoxic event, show de-oxygenation below the mean levels observed in the Angola waters located north of the glider (Figure 6), despite maintaining a match in salinity with these waters, possibly indicating a different history of biogeochemical transformations of the associated water.

3.5 Oxygen variability: mesoscale drivers

We focus here on P2 and P3, illustrating two distinct mesoscale processes captured by the glider data and affecting the oxygen distribution in the offshore northern BenUS. These also correspond to some of the shallowest and most intense hypoxic events observed during the glider campaign.

3.5.1 Phase 2: severe hypoxia associated with the undercurrent intensification and the likely spinning of a subsurface eddy

P2 (17/March - 13/April) is characterised by visible surface poleward flow along the BenUS shelf and by minimum lateral flow at the glider position (Figure 2d-f,m). Despite the relatively calm surface water conditions, a sharp and persistent hypoxic event spans the depth range between 75 m and 300 m for about one week between 27/March (when the glider reaches measurement spot BN) and 03/April, hosting significant domains of severe hypoxia (Figure 5, P2). In addition to concurrent positive temperature and salinity anomalies, the hypoxic event is associated with a deep bulging of the isopycnals (Figure 3, P2), and a local minimum in the Brunt-Väisälä frequency (N^2), especially between 200 and 300 m depth (see Supplement Figure S7c,S10d). This set of properties is characteristic of subsurface anticyclonic eddies, previously observed in upwelling regions and often shed by the shelf undercurrents carrying low oxygen waters (Frenger et al., 2018; Molemaker et al., 2015). As satellite SST for P2 indicates the presence of an active poleward transport of warm and potentially deoxygenated tropical water along the BenUS shelf (Figure 2f), this hypothesis is especially likely. We must note that the N^2 minimum is not as clear as expected for a sub-surface eddy structure, and it shows only a limited signature of a sharp peripheral maximum that would indicate the lateral isolation of the eddy core. This potentially indicates that the detected structure may still be unstable or in formation (see further discussion in subsection 4.2). The Tc - Sa diagram for P2, however, shows a clear separation between hypoxic and oxygenated waters (Figure 8a), indicating a sharp transition between SACW and ESACW and therefore weak mixing between water masses, which is not observed in the other phases (Figure 8b, see also Supplement Figure S12).

We therefore infer that the detected structure is most likely a subsurface anticyclone spinning from the undercurrent. This structure combines extreme hypoxic conditions with a lack of a surface signature, which makes it impossible to detect from satellite data. Further, the limited lateral mixing between the water within and outside of the structure, as indicated by the separation of water masses in the T_c-S_a diagram for P2, results in a sharp but transitory pattern of hypoxia and severe hypoxia. Minimum O_2 concentrations in this structure recurrently fall below 20 µmol kg^{-1} and reach as low as 16 µmol kg^{-1}. Such oxygen concentrations are lower than the climatological mean observed for the water mass located north of the glider (Figure 6, P2); this anomaly also corresponds to a dip in particle concentrations (see Supplement Figure S7a, P2). Both signatures suggest that, compared to the surrounding waters, this water was subject to higher levels of remineralisation, possibly occurring on the shelf. The largest spatial gradients at the edge of the anomaly were found between 200 and 400 m depth, with oxy-

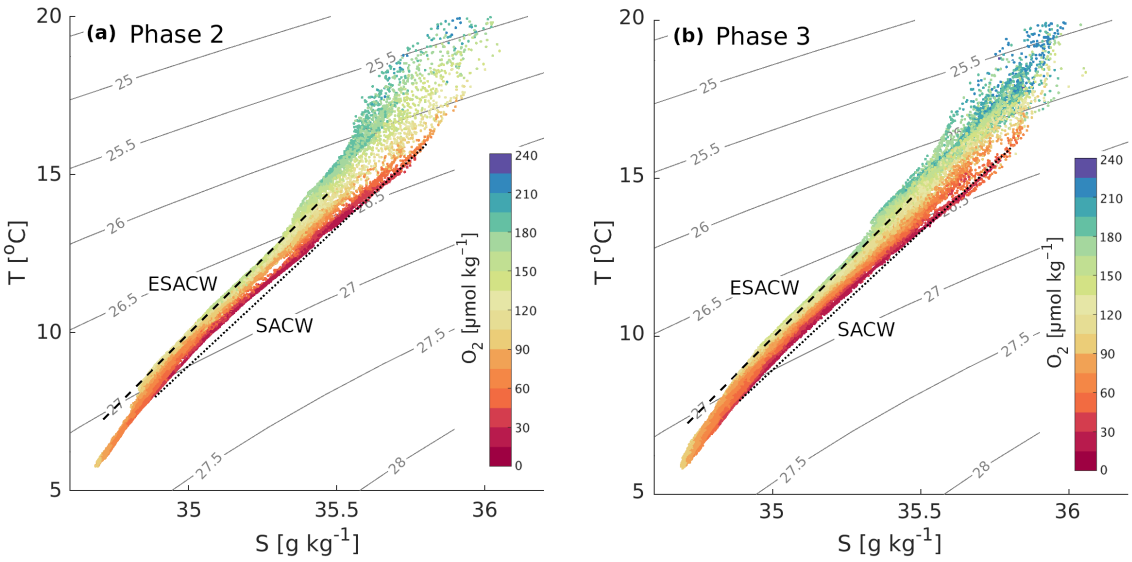

Figure 8. Conservative temperature (T_c) and absolute salinity (S_a) diagram of the binned glider data restricted to the range of 50-600 m depth during (a) phase 2 (17/March - 13/April), and (b) phase 3 (16/April - 31/May). Dots are coloured according to oxygen concentration, density isolines are plotted in gray [kg m^{-3}]. The characteristic T_c-S_a trends of SACW and ESACW are highlighted respectively by a dotted and a dashed black line. Full-depth diagrams for the 4 phases can be found in Supplement Figure S12.

gen concentrations varying by between 30 and 40 µmol kg^{-1} km^{-1}. Given that the glider was sampling along a triangle of 12 km per side, the diameter of the structure must have been larger than about 16 km in order to be sampled continuously for a week's time - however, we are unable to estimate the full size of the structure and therefore to evaluate whether it was in the meso- or submesoscale range.

3.5.2 Phase 3: stirring at the rim of a large frontal anticyclone

During P3 (16/April - 31/May), the glider is located in a region of intense lateral surface flow, i.e., at the rim of a large anticyclone that stirs northern offshore Angola water and southern Benguela water across the ABFZ (Figure 2g-i,m, Figure S1). Satellite images show that from late April to mid-May (eddy formation and intensification phases) the glider crosses fronts between northern warm&low-CHL water and cold&high-CHL water from the nearshore Benguela. This emerges as strong variations in physical properties both within the mixed layer and at depth (Figure 3, P3), and in oxygen concentrations at depths of 100 m - 500 m (Figure 5, P3). Oxygen within the mixed layer, instead, is dominated by fast air-sea exchange fluxes. A fine pattern of concurrent fluctuations in T_c, S_a and O_2 persists across May, especially at depths of 100 - 500 m, indicating that the glider is crossing very sharp gradients between water masses. During this period, spatial gradients in the O_2 concentrations exceed 50 µmol kg^{-1} km^{-1}. These small scale patterns and the lack of separation between water masses shown by the T_c-S_a diagram for P3 (Figure 8b) suggests that eddy stirring is enhancing mixing between water masses. This is also suggested by the difference plots between S_a and O_2 and the water mass properties north and south of the glider, which also show intermediate salinity and oxygen concentrations in early May (Figure 6, P3).

In the second half of May, the eddy detaches from the coast to move offshore (see Supplement Figure S1). Glider data show a progressive switch from a prevalence of ESACW to SACW, and fronts start to be associated with sporadic severe hypoxia at depths of 250 - 450 m, a fine pattern that is not as shallow nor as persistent as the one observed during P2. Mid to late May also sees an intensification of coastal upwelling with intense bursts in late May - early June (see Supplement Figure S2a), corresponding to oxygen concentrations falling below the climatological mean of the northern water mass at depths of 100 m - 200 m (Figure 6, P3-P4). The fine-scale pattern observed in late May is likely to result from a combination of anticyclonic stirring, upwelling intensification bringing low-oxygen shelf water towards the glider position and a reactivation of the alongshore poleward transport of SACW subsequent to the offshore drift of the eddy.

4 Discussion

4.1 Physics driving oxygen variability in the offshore northern Benguela

The results of our manuscript show that, at the latitudes of the measurements, physical processes in the form of alternating lateral fluxes of SACW and ESACW are the dominant drivers of sub-monthly fluctuations in the oxygen availability between 100 m and 500 m depth in the offshore northern Benguela. Hypoxia at the glider location can't be explained only by a combination of sluggish ventilation and local biological uptake of organic material. These observations extend to offshore waters the findings of previous studies highlighting that physical processes, in the form of lateral fluxes of hypoxic SACW waters, are the primary driver of hypoxia and the main trigger of the onset of anoxia (near-zero oxygen concentrations) on the shelf of the BenUS (Monteiro et al., 2006, 2008). Although anoxia is not observed in our dataset, both hypoxia and severe hypoxia emerge from the lateral influx of SACW, as suggested by the analysis of the T_c-S_a signatures and a comparison with the climatological offshore Angola and Benguela oxygen and salinity profiles. More oxygenated conditions, on the other hand, are associated to an inflow of intermediate waters with T_c-S_a signature characteristic of the southern-derived ESACW. The observed magnitude and temporal scale of variability in oxygen also suggests that datasets aiming to resolve monthly means and long-term oxygen trends in the offshore northern Benguela should account for such sub-monthly fluctuations and make sure to adopt a statistically significant set of measurements in order not to incur in biases. Continuous and long-term observations are of great value to account for the observed variability and to correctly resolve the monthly mean oxygen profile in the open waters of the northern BenUS.

The signatures of SACW and ESACW at 100 m - 350 m depth alternate with each other on the timescale of one to two weeks at the glider position, while SACW seems more persistent at deeper depths. Only some of these anomalies can be associated with mesoscale features. Modeling studies by Muller et al. (2014); Schmidt and Eggert (2016) show that, in austral summer, the shelf undercurrent at 18°S deepens to about 200 m - 400 m depth in the offshore region of the system. Most of the observed fluctuations may therefore be associated with short-lived pulses of the shelf undercurrent reaching the offshore region of the northern Benguela and carrying water from the north, which may determine an intensification and/or wider depth range of the poleward transport. Variability in temperature, salinity and oxygen on the scale of a few days to two weeks was also observed by Monteiro et al. (2006) on the BenUS shelf at 23°S. The oxygen variability on the shelf and in the subsurface off-shore northern BenUS region may therefore be modulated on similar temporal scales. Studies showed that coastal trapped waves generated by wind stress forcing within the BenUS oscillate with a period of a few days to weeks (Junker et al., 2019), and may therefore contribute to the variability of the transport of SACW along the shelf at the latitude of the glider.

4.2 Mesoscale drivers

On top of the large-scale circulation, mesoscale activity impacts oxygen concentration at the glider position. We identify two mesoscale processes that affect the oxygen variability at the time of sampling: lateral advection of severely hypoxic water most likely by a subsurface anticyclone during an intensification of the undercurrent (P2), and cross-frontal stirring by a large anticyclone (P3). While the structure associated with P3 is identifiable from surface satellite data, this is not the case for P2. Since glider measurements at BN were collected at roughly 95 km from the BenUS coast, a subsurface eddy spinning from the shelf undercurrent is likely to be young or in formation at such a limited offshore distance (Thomsen, Kanzow, Krahmann, et al., 2016) and possibly still unstable, which could explain the weak N^2 signature. This is also suggested by observing the lateral extension of multiple forming anticyclonic loops in model reanalysis data during the undercurrent intensification of P2 (see GLORYS12v1 reanalysis data in Supplement Figure S4). It is also unlikely that the glider sampled continuously at the very center of the eddy core, resulting in a higher degree of noise in N^2. A detailed analysis of the glider position for each profile indicates that the glider may have entered and exited the structure from the same southern side, and moved along the triangular sampling path within its perimeter for the duration of the anomaly. Alternative hypotheses, such as the anomaly being associated with poleward laminar transport by the undercurrent flowing off the shelf rather than an eddy spinning off the shelf portion of the current, would not be able to explain the shape of the isopycnals nor the especially low oxygen and particle concentrations of P2 compared to the other observed hypoxic events (Figure 6b and Supplement Figure S7a). Anticyclonic eddies shed by subsurface currents, in fact, are known to trap and advect extremely low oxygen shelf water (Frenger et al., 2018), while high remineralization rates in well-isolated subsurface eddy cores can further exacerbate low oxygen conditions (Karstensen et al., 2015, 2017). The anomaly being associated to a precursor of an actual eddy, such as instabilities in the flow of the subsurface current (Molemaker et al., 2015), is also unlikely due to the anomalies suggesting some degree of coherence and isolation in the structure. Small scale laminar transport from the coast, e.g., upwelling filament transport, cannot explain the sluggish flow observed during the anomaly in velocity products (Figure 2m) nor the deep signature of the structure, as filaments are typically confined to the upper 100 m (Cravo et al., 2010; Thomsen, Kanzow, Colas, et al., 2016).

Surface and subsurface eddies are an intrinsic mode of flow in upwelling systems (Chaigneau et al., 2009; Frenger et al., 2018). The mesopelagic oxygen field in the sampled region is therefore recurrently impacted by their associated oxygen signature, fine scale patchiness and water mass mixing. Subsurface eddies in the BenUS were previously detected in Argo temperature and salinity profiles (McCoy et al., 2020), however, to our knowledge, hypoxia within a subsurface eddy shedding from the BenUS undercurrent has not previously been observed in situ. There is an abundance of literature studying the physical properties and biogeochemistry of such eddies in other upwelling systems based on in-situ and model data (e.g., Chaigneau et al. (2011); Schütte et al. (2016b); Fiedler et al. (2016); Karstensen et al. (2017); Frenger et al. (2018); Auger et al. (2021)) which have found that low-oxygen anomalies trapped and further intensified within subsurface eddies generated along the shelf are transported towards the middle of the gyre, where they shape the large-scale oxygen gradient of mid-latitudes. In the tropical North Atlantic, a satellite-based study estimated these structures constituted 9% of the eddy population (Schütte et al., 2016a). However, additional preliminary work based on models suggests a remarkably higher ratio of subsurface eddies globally (40 % of all the eddies), with most (75%) showing no surface signature (Schütte et al., EGU2021, talk), therefore suggesting an even more significant impact on biogeochemical fields.

Large frontal eddies such as the one observed in P3 are also known to be a recurrent feature of the ABFZ (Boyer et al., 2000). The fine-scale T_c, S_a and O_2 patterns (Fig-

ures 3,5) and the intermediate salinity and oxygen properties (Figure 6,8) observed in mid May indicate that such cross-frontal anticyclones are an effective means through which SACW and ESACW mix at the ABFZ and that, as a result, such eddies smooth the cross-frontal tracer gradients. From the perspective of the Angola region, this lateral stirring is likely to ventilate the South Atlantic OMZ by laterally advecting and stirring higher oxygen concentrations into the northern latitudes, similar to what is observed for example in the North Atlantic (Kolodziejczyk et al., 2018).

4.3 Seasonality and future trends

Seasonality is expected to play a role in our results. Glider measurements were collected between February and June, i.e. during the low upwelling season characterised by minimum O_2 levels on the BenUS shelf and frequent intrusions of tropical water (Boyer et al., 2000). With the onset of the austral winter-spring upwelling season, more oxygenated and nutrient-rich waters are brought onto the shelf (Monteiro et al., 2008; Mohrholz et al., 2008), possibly resulting in less frequent, weaker and/or more confined hypoxic events at the measurement site. Although our glider measurements do not fully capture seasonal variability, the data show changes in all tracers approaching June, i.e., towards the beginning of winter (Figures 3,5). With the onset of upwelling, during late P3 and P4 (see Supplement Figure S2a), glider data show that low oxygen anomalies are confined within a narrower range of depths, between 200 m and 400 m. During the upwelling season, the offshore BenUS may therefore be characterised by even sharper O_2 gradients between different depths. Phases characterised by active upwelling (late P3-P4 and, to a lesser extent, P1) also present some severe hypoxic concentrations, although the signals are not as persistent as during P2. In the case of shallow and short-lived severe hypoxic events such as the one emerging at the very end of P3, this may be possibly linked to some low-oxygen shelf water being advected offshore towards the glider. Longer lasting severe hypoxic events observed during the upwelling intensification, such as the one observed during June (P4) between 300-400 m, are deeper than the one detected during P2 and therefore fall close to the climatological O_2 profile of the northern SACW (Figure 6b). Longer data series and model studies are needed in order to better decouple the role of the southward and offshore transport of low oxygen water during periods of intensified upwelling. Longer term data are also needed to collect enough statistics of these oxygen fluctuations and understand how seasonal changes in currents and biological activity affect their duration and depth distribution.

This study further highlights the strong lateral coupling between the biogeochemistry of Angola and Benguela, which extends beyond the shelf region into the open waters. The recent and future expansion of the ocean's OMZs, including the Angola OMZ, constitutes a significant risk for ecosystems and fisheries in upwelling regions (Bopp et al., 2013; Keeling et al., 2010; Bograd et al., 2023). As oxygen levels fall, hypoxic events will become more probable, shrinking the habitable range for many marine species (Breitburg et al., 2018; Gilly et al., 2013). Observations suggest that in the equatorial Atlantic oxygen concentrations have largely declined in the last decades, falling by about -5 µmol kg^{-1} at a depth of 300 m over the last 50 years (Schmidtko et al., 2017). Lower oxygen levels in the Angola region are likely to impact the offshore northern BenUS, with pulses of undercurrent likely transporting increasingly deoxygenated shelf waters and frontal eddies stirring more severe low oxygen anomalies into more southerly latitudes, and possibly also across a wider range of depths. Furthermore, our results highlight that the impact of large scale changes in oxygen concentrations on the offshore northern Benguela will depend also on the future evolution of the physical fluxes coupling the this region with the southern Benguela latitudes and with the Angola. Eddy-resolving coupled physical-biological model simulations are needed to better understand these trends and their potential impact on the local ecosystem.

4.4 Implications for marine organisms

Our results provide information on the extension of the habitable depth range for different marine species in the offshore northern BenUS and can provide useful data to better understand their metabolic and behavioural adaptation to the local oxygen variability and the spatial patchiness and temporal intermittency of hypoxia. Hypoxic events ($O_2 < 60$ µmol kg^{-1}) during our deployment period were confined between 68 m and 546 m depth, with a probability of occurrence exceeding 10 % at 100 m depth, i.e., just beneath the most productive layer. These events, although intermittent in time, constitute significant stressors for marine organisms and can strongly modulate the ecosystem behaviour (Gilly et al., 2013; Eby et al., 2005; Vaquer-Sunyer & Duarte, 2008; Keppel et al., 2016). Spatial and temporal patchiness in oxygenation can create niches for hypoxia-resistant organisms as well as force sensitive species to migrate, thus modulating the coupling between different trophic levels, and potentially forcing prey closer to their predators or predators away from their prey (Breitburg, 2002; Bell & Eggleston, 2005). Since severe hypoxia is confined to a depth range narrower than that of hypoxia, organisms that can tolerate very low oxygen levels, such as copepods, gelatinous plankton and squids, have the potential to occupy a larger habitable zone not only in the near surface but also at depth (Ekau et al., 2010; Gilly et al., 2013). Sub-lethal oxygen levels ($O_2 < 120$ µmol kg^{-1}), on the other hand, become increasingly more probable with depth up to ∼700 m depth. This implies that organisms that are extremely sensitive to low oxygen, such as crustaceans and fish larvae, are likely confined within the mixed layer, while many fish species sensitive to sub-lethal oxygen thresholds in this range may alter their metabolism in order to inhabit a wider range of depths (Vaquer-Sunyer & Duarte, 2008).

5 Conclusions and outlook

In the present study we discussed the temporal variability of oxygen concentrations in the offshore northern BenUS using high-resolution glider data collected between February and June 2018. Our results show that weekly alternating fluxes of tropical SACW and southern ESACW are the primary driver of the significant O_2 fluctuations in the upper mesopelagic. Hypoxic events are connected to the presence of tropical water and are intermittent in time, rarely exceeding one week's duration in the range of 100-300 m depth, revealing significant variability in the pattern of subsurface fluxes at the ABFZ. Further, we demonstrated the key role of the mesoscale subsurface transport from the shelf and mesoscale lateral stirring across the ABFZ in driving severe hypoxia, subsurface oxygen patchiness and water mass mixing at the Angola-Benguela front.

Our results underline the importance of continuous and high-resolution observations in the offshore region of the northern Benguela, in order to better characterise the observed oxygen variability and correctly resolve its mean. Longer time series of in-situ data and modeling studies are needed to clarify how frequency, duration, intensity and spatial patterns of both hypoxic events and the driving SACW/ESACW subsurface fluxes vary with seasons and on interannual time scales. The role of local biology in further modulating the detected low oxygen anomalies should also be clarified, including addressing the consequences for particle concentrations and export during hypoxic events. The effect of intermittent hypoxia on organisms and ecosystem structure of upwelling regions also needs further investigation (Eby et al., 2005; Keppel et al., 2016), especially with regards to diel vertical migrators, which might be particularly impacted by the observed subsurface advection of hypoxic water. Further, modeling studies can also help to understand how hypoxia variability and prevalence in the northern BenUS will evolve in the context of future changes as a result of the region's lateral coupling with both the South Atlantic OMZ and the southern Benguela (Breitburg et al., 2018; Gilly et al., 2013).

Acknowledgments

We would like to thank Dr Alice Della Penna, Dr Evan Mason and Dr Ivy Frenger for their valuable input and feedback. Further thanks go to Dr Anja Van Der Plas and Dr Giulia Bonino for their precious suggestions. We also thank the 4 anonymous reviewers for their time and feedback. This research was financially supported by the Swiss National Science Foundation (SNSF grant number P2EZP2_184251). This work was supported by a European Research Council Consolidator grant (GOCART, agreement number 724416) and the Natural Environment Research Council through the COMICS project (Controls over Ocean Mesopelagic Interior Carbon Storage; NE/M020835/1). The authors declare that they have no conflict of interest. The data "Northern Benguela glider dataset, February-June 2018 (temperature, salinity, density, dissolved oxygen, 1000m depth-averaged and surface currents)" can be accessed and downloaded at:
https://doi.pangaea.de/10.1594/PANGAEA.938221
Oceanographic quantities were converted using the TEOS-10 Gibbs Seawater (GSW) Oceanographic Toolbox (McDougall & Barker, 2011). Figures were produced using standard built-in functions of MATLAB (pcolor, contour, scatter, plot) and the M_Map mapping package for MATLAB (Pawlowicz, 2020).

References

Auger, P. A., Bento, J. P., Hormazabal, S., Morales, C. E., & Bustamante, A. (2021). Mesoscale variability in the boundaries of the oxygen minimum zone in the eastern south pacific: Influence of intrathermocline eddies. *Journal of Geophysical Research: Oceans*, *126*(2), e2019JC015272. Retrieved from `https://agupubs.onlinelibrary.wiley.com/doi/abs/10.1029/2019JC015272` (e2019JC015272 2019JC015272) doi: https://doi.org/10.1029/2019JC015272

Bachèlery, M.-L., Illig, S., & Rouault, M. (2020). Interannual coastal trapped waves in the angola-benguela upwelling system and benguela nio and nia events. *Journal of Marine Systems*, *203*, 103262. Retrieved from `https://www.sciencedirect.com/science/article/pii/S0924796319303999` doi: https://doi.org/10.1016/j.jmarsys.2019.103262

Bartholomae, C., & van der Plas, A. (2007). Towards the development of environmental indices for the namibian shelf, with particular reference to fisheries management. *African Journal of Marine Science*, *29*(1), 25-35. Retrieved from `https://doi.org/10.2989/AJMS.2007.29.1.2.67` doi: 10.2989/AJMS.2007.29.1.2.67

Bell, G., & Eggleston, D. (2005). Species-specific avoidance responses by blue crabs and fish to chronic and episodic hypoxia. *Marine Biology*, *146*(4), 761–770.

Bograd, S. J., Jacox, M. G., Hazen, E. L., Lovecchio, E., Montes, I., Pozo Buil, M., ... Rykaczewski, R. R. (2023). Climate change impacts on eastern boundary upwelling systems. *Annual Review of Marine Science*, *15*(1), null. Retrieved from `https://doi.org/10.1146/annurev-marine-032122-021945` (PMID: 35850490) doi: 10.1146/annurev-marine-032122-021945

Bopp, L., Resplandy, L., Orr, J. C., Doney, S. C., Dunne, J. P., Gehlen, M., ... Vichi, M. (2013). Multiple stressors of ocean ecosystems in the 21st century: projections with cmip5 models. *Biogeosciences*, *10*(10), 6225–6245. Retrieved from `https://bg.copernicus.org/articles/10/6225/2013/` doi: 10.5194/bg-10-6225-2013

Boyer, D., Cole, J., & Bartholomae, C. (2000). Southwestern africa: Northern benguela current region. *Marine Pollution Bulletin*, *41*(1), 123-140. Retrieved from `https://www.sciencedirect.com/science/article/pii/S0025326X00001065` (Seas at the Millennium: an Environmental Evaluation) doi: https://doi.org/10.1016/S0025-326X(00)00106-5

Brandt, P., Bange, H. W., Banyte, D., Dengler, M., Didwischus, S.-H., Fischer, T., ... Visbeck, M. (2015). On the role of circulation and mixing in the

ventilation of oxygen minimum zones with a focus on the eastern tropical north atlantic. *Biogeosciences*, *12*(2), 489–512. Retrieved from https://bg.copernicus.org/articles/12/489/2015/ doi: 10.5194/bg-12-489-2015

Breitburg, D. (2002). Effects of hypoxia, and the balance between hypoxia and enrichment, on coastal fishes and fisheries. *Estuaries*, *25*(4), 767–781.

Breitburg, D., Levin, L. A., Oschlies, A., Grégoire, M., Chavez, F. P., Conley, D. J., ... Zhang, J. (2018). Declining oxygen in the global ocean and coastal waters. *Science*, *359*(6371). Retrieved from https://science.sciencemag.org/content/359/6371/eaam7240 doi: 10.1126/science.aam7240

Carr, M.-E., & Kearns, E. J. (2003, November-December). Production regimes in four eastern boundary current systems. *Deep-Sea Research II*, *50*(22-26), 3199-3221. doi: http://dx.doi.org/10.1016/j.dsr2.2003.07.015

Chaigneau, A., Eldin, G., & Dewitte, B. (2009). Eddy activity in the four major upwelling systems from satellite altimetry (19922007). *Progress in Oceanography*, *83*(1), 117 - 123. Retrieved from http://www.sciencedirect.com/science/article/pii/S0079661109001013 (Eastern Boundary Upwelling Ecosystems: Integrative and Comparative Approaches) doi: http://dx.doi.org/10.1016/j.pocean.2009.07.012

Chaigneau, A., Le Texier, M., Eldin, G., Grados, C., & Pizarro, O. (2011). Vertical structure of mesoscale eddies in the eastern south pacific ocean: A composite analysis from altimetry and argo profiling floats. *Journal of Geophysical Research: Oceans*, *116*(C11), n/a–n/a. Retrieved from http://dx.doi.org/10.1029/2011JC007134 (C11025) doi: 10.1029/2011JC007134

Chavez, F. P., & Messié, M. (2009, December). A comparison of eastern boundary upwelling ecosystems. *Progress in Oceanography*, *83*(1-4), 80-96. doi: http://dx.doi.org/10.1016/j.pocean.2009.07.032

CMEMS. (2020). *Global ocean chlorophyll, pp and pft (copernicus-globcolour) from satellite observations: Monthly and daily interpolated (reprocessed from 1997)* (Tech. Rep.). E.U. Copernicus Marine Service Information. doi: https://doi.org/10.48670/moi-00100

CMEMS. (2022). *Global ocean gridded l4 sea surface heights and derived variables reprocessed (1993-ongoing)* (Tech. Rep.). E.U. Copernicus Marine Service Information, SEALEVEL_GLO_PHY_L4_MY_008_047. Retrieved from https://doi.org/10.48670/moi-00148 (https://catalogue.marine.copernicus.eu/documents/PUM/CMEMS-SL-PUM-008-032-068.pdf, Accessed: 06 Apr 2022)

Cravo, A., Relvas, P., Cardeira, S., Rita, F., Madureira, M., & Snchez, R. (2010). An upwelling filament off southwest iberia: Effect on the chlorophyll a and nutrient export. *Continental Shelf Research*, *30*(15), 1601 - 1613. Retrieved from http://www.sciencedirect.com/science/article/pii/S0278434310002001 doi: http://dx.doi.org/10.1016/j.csr.2010.06.007

Crocker, R. I., Matthews, D. K., Emery, W. J., & Baldwin, D. G. (2007). Computing coastal ocean surface currents from infrared and ocean color satellite imagery. *IEEE Transactions on Geoscience and Remote Sensing*, *45*(2), 435-447. doi: 10.1109/TGRS.2006.883461

Diakhaté, M., de Cotlogon, G., Lazar, A., Wade, M., & Gaye, A. T. (2016). Intraseasonal variability of tropical atlantic sea-surface temperature: airsea interaction over upwelling fronts. *Quarterly Journal of the Royal Meteorological Society*, *142*(694), 372-386. Retrieved from https://rmets.onlinelibrary.wiley.com/doi/abs/10.1002/qj.2657 doi: https://doi.org/10.1002/qj.2657

Drévillon, M., Regnier, C., Lellouche, J., Garric, G., Bricaud, C., & Hernandez, O. (2018). *Cmems quality information document for global ocean reanalysis product, cmems-glo-quid-001-030, 1.2 edn.* (Tech. Rep.). E.U. Copernicus Marine Service Information [Online]. Retrieved from https://resources

.marine.copernicus.eu/documents/QUID/CMEMS-GLO-QUID-001-030.pdf ((Accessed: 19 January 2021))

Eby, L. A., Crowder, L. B., McClellan, C. M., Peterson, C. H., & Powers, M. J. (2005). Habitat degradation from intermittent hypoxia: impacts on demersal fishes. *Marine Ecology Progress Series*, *291*, 249–262.

Ekau, W., Auel, H., Pörtner, H.-O., & Gilbert, D. (2010). Impacts of hypoxia on the structure and processes in pelagic communities (zooplankton, macro-invertebrates and fish). *Biogeosciences*, *7*(5), 1669–1699. Retrieved from https://bg.copernicus.org/articles/7/1669/2010/ doi: 10.5194/bg-7-1669-2010

Faghmous, J. H., Frenger, I., Yao, Y., Warmka, R., Lindell, A., & Kumar, V. (2015). A daily global mesoscale ocean eddy dataset from satellite altimetry. *Scientific Data*, *2*. Retrieved from http://dx.doi.org/10.1038/sdata.2015.28

Fennel, K., & Testa, J. M. (2019). Biogeochemical controls on coastal hypoxia. *Annual Review of Marine Science*, *11*(1), 105-130. Retrieved from https://doi.org/10.1146/annurev-marine-010318-095138 (PMID: 29889612) doi: 10.1146/annurev-marine-010318-095138

Fernandez, E., & Lellouche, J. (2018). *Product user manual for the global ocean physical reanalysis product global_reanalysis_phy_001_030.* (E.U. Copernicus Marine Service Information (data set) Global Monitoring and Forecasting Center GLORYS12V1 - Global Ocean Physical Reanalysis Product (Accessed: 19 January 2021))

Fiedler, B., Grundle, D. S., Schütte, F., Karstensen, J., Löscher, C. R., Hauss, H., ... Körtzinger, A. (2016). Oxygen utilization and downward carbon flux in an oxygen-depleted eddy in the eastern tropical north atlantic. *Biogeosciences*, *13*(19), 5633–5647. Retrieved from https://bg.copernicus.org/articles/13/5633/2016/ doi: 10.5194/bg-13-5633-2016

Flohr, A., van der Plas, A. K., Emeis, K.-C., Mohrholz, V., & Rixen, T. (2014). Spatio-temporal patterns of c : N : P ratios in the northern benguela upwelling system. *Biogeosciences*, *11*(3), 885–897. Retrieved from https://bg.copernicus.org/articles/11/885/2014/ doi: 10.5194/bg-11-885-2014

Frenger, I., Bianchi, D., Sthrenberg, C., Oschlies, A., Dunne, J., Deutsch, C., ... Schtte, F. (2018). Biogeochemical role of subsurface coherent eddies in the ocean: Tracer cannonballs, hypoxic storms, and microbial stewpots? *Global Biogeochemical Cycles*, *32*(2), 226-249. Retrieved from https://agupubs.onlinelibrary.wiley.com/doi/abs/10.1002/2017GB005743 doi: https://doi.org/10.1002/2017GB005743

Garcia, H., Boyer, T., Baranova, O., Locarnini, R., Mishonov, A., Grodsky, A., ... Zweng, M. (2019). *World ocean atlas 2018: Product documentation (a. mishonov, technical editor)* (Tech. Rep.). NOAA/NESDIS National Centers for Environmental Information. Retrieved from https://www.ncei.noaa.gov/data/oceans/woa/WOA18/DOC/woa18documentation.pdf ((Accessed: 19 January 2021))

Garçon, V., Dewitte, B., Montes, I., & Goubanova, K. (2019). Land-sea-atmosphere interactions exacerbating ocean deoxygenation in eastern boundary upwelling systems (ebus). In D. Laffoley & J. M. Baxter (Eds.), *Ocean deoxygenation: Everyone's problem-causes, impacts, consequences and solutions.* IUCN Gland, Switzerland.

GEBCO. (2019). *General bathymetric chart of the oceans (gebco)* (Tech. Rep.). Retrieved from https://www.gebco.net/data_and_products/gridded_bathymetry_data/gebco_2019/gebco_2019_info.html

Gibson, R., & Atkinson, R. (2003). Oxygen minimum zone benthos: adaptation and community response to hypoxia. *Oceanogr. Marine Biol. Annu. Rev*, *41*, 1–45.

Gilly, W. F., Beman, J. M., Litvin, S. Y., & Robison, B. H. (2013). Oceanographic

and biological effects of shoaling of the oxygen minimum zone. *Annual review of marine science*, *5*, 393–420.

Good, S., Fiedler, E., Mao, C., Martin, M. J., Maycock, A., Reid, R., ... Worsfold, M. (2020). The current configuration of the ostia system for operational production of foundation sea surface temperature and ice concentration analyses. *Remote Sensing*, *12*(4). Retrieved from https://www.mdpi.com/2072-4292/12/4/720 (CMEMS E.U. Copernicus Marine Service Information, SST_GLO_SST_L4_REP_OBSERVATIONS_010_011, data doi: https://doi.org/10.48670/moi-00168 Accessed: 06 Apr 2022) doi: 10.3390/rs12040720

Grantham, B. A., Chan, F., Nielsen, K. J., Fox, D. S., Barth, J. A., Huyer, A., ... Menge, B. A. (2004). Upwelling-driven nearshore hypoxia signals ecosystem and oceanographic changes in the northeast pacific. *Nature*, *429*(6993), 749–754.

Hardman-Mountford, N., Richardson, A., Agenbag, J., Hagen, E., Nykjaer, L., Shillington, F., & Villacastin, C. (2003). Ocean climate of the south east atlantic observed from satellite data and wind models. *Progress in Oceanography*, *59*(2), 181-221. Retrieved from https://www.sciencedirect.com/science/article/pii/S007966110300168X (ENVIFISH: Investigating environmental causes of pelagic fisheries variability in the SE Atlantic) doi: https://doi.org/10.1016/j.pocean.2003.10.001

Hersbach, H., Bell, B., Berrisford, P., Hirahara, S., Hornyi, A., Muoz-Sabater, J., ... Thpaut, J.-N. (2020). The era5 global reanalysis. *Quarterly Journal of the Royal Meteorological Society*, *146*(730), 1999-2049. Retrieved from https://rmets.onlinelibrary.wiley.com/doi/abs/10.1002/qj.3803 doi: https://doi.org/10.1002/qj.3803

Hu, L., Zhang, X., & Perry, M. J. (2019). Light scattering by pure seawater: Effect of pressure. *Deep Sea Research Part I: Oceanographic Research Papers*, *146*, 103-109. Retrieved from https://www.sciencedirect.com/science/article/pii/S0967063719300226 doi: https://doi.org/10.1016/j.dsr.2019.03.009

Hutchings, L., van der Lingen, C., Shannon, L., Crawford, R., Verheye, H., Bartholomae, C., ... Monteiro, P. (2009). The benguela current: An ecosystem of four components. *Progress in Oceanography*, *83*(1), 15-32. Retrieved from https://www.sciencedirect.com/science/article/pii/S0079661109001104 (Eastern Boundary Upwelling Ecosystems: Integrative and Comparative Approaches) doi: https://doi.org/10.1016/j.pocean.2009.07.046

Illig, S., & Bachèlery, M.-L. (2019). Propagation of subseasonal equatorially-forced coastal trapped waves down to the benguela upwelling system. *Scientific reports*, *9*(1), 1–10.

Imbol Koungue, R. A., Brandt, P., Lbbecke, J., Prigent, A., Martins, M. S., & Rodrigues, R. R. (2021). The 2019 benguela nio. *Frontiers in Marine Science*, *8*. Retrieved from https://www.frontiersin.org/article/10.3389/fmars.2021.800103 doi: 10.3389/fmars.2021.800103

Ito, T., Minobe, S., Long, M. C., & Deutsch, C. (2017). Upper ocean o2 trends: 19582015. *Geophysical Research Letters*, *44*(9), 4214-4223. Retrieved from https://agupubs.onlinelibrary.wiley.com/doi/abs/10.1002/2017GL073613 doi: https://doi.org/10.1002/2017GL073613

John, H.-C., Zelck, C., & Erasmi, W. (2000). Poleward transport of equatorial fish larvae in the atlantic eastern boundary current system. *Archive of Fishery and Marine Research*, *48*(1), 61–88. Retrieved from http://eprints.uni-kiel.de/4784/

Junker, T., Mohrholz, V., Schmidt, M., Siegfried, L., & van der Plas, A. (2019). Coastal trapped wave propagation along the southwest african shelf as revealed by moored observations. *Journal of Physical Oceanography*, *49*(3), 851 - 866.

Retrieved from https://journals.ametsoc.org/view/journals/phoc/49/3/jpo-d-18-0046.1.xml doi: 10.1175/JPO-D-18-0046.1

Kainge, P., Kirkman, S. P., Estevo, V., van der Lingen, C. D., Uanivi, U., Kathena, J. N., ... Hamukuaya, H. (2020). Fisheries yields, climate change, and ecosystem-based management of the benguela current large marine ecosystem. *Environmental Development*, *36*, 100567. Retrieved from https://www.sciencedirect.com/science/article/pii/S2211464520300890 (Large Marine Ecosystems of Africa: Assessment, Sustainability, and Management) doi: https://doi.org/10.1016/j.envdev.2020.100567

Kara, A. B., Rochford, P. A., & Hurlburt, H. E. (2003). Mixed layer depth variability over the global ocean. *Journal of Geophysical Research: Oceans*, *108*(C3). Retrieved from https://agupubs.onlinelibrary.wiley.com/doi/abs/10.1029/2000JC000736 doi: https://doi.org/10.1029/2000JC000736

Karstensen, J., Fiedler, B., Schütte, F., Brandt, P., Körtzinger, A., Fischer, G., ... Wallace, D. (2015). Open ocean dead zones in the tropical north atlantic ocean. *Biogeosciences*, *12*(8), 2597–2605. Retrieved from http://www.biogeosciences.net/12/2597/2015/ doi: 10.5194/bg-12-2597-2015

Karstensen, J., Schütte, F., Pietri, A., Krahmann, G., Fiedler, B., Grundle, D., ... Visbeck, M. (2017). Upwelling and isolation in oxygen-depleted anticyclonic modewater eddies and implications for nitrate cycling. *Biogeosciences*, *14*(8), 2167–2181. Retrieved from https://www.biogeosciences.net/14/2167/2017/ doi: 10.5194/bg-14-2167-2017

Karstensen, J., Stramma, L., & Visbeck, M. (2008). Oxygen minimum zones in the eastern tropical atlantic and pacific oceans. *Progress in Oceanography*, *77*(4), 331-350. Retrieved from https://www.sciencedirect.com/science/article/pii/S0079661108000670 (A New View of Water Masses After WOCE. A Special Edition for Professor Matthias Tomczak) doi: https://doi.org/10.1016/j.pocean.2007.05.009

Keeling, R. F., Krtzinger, A., & Gruber, N. (2010). Ocean deoxygenation in a warming world. *Annual Review of Marine Science*, *2*(1), 199-229. Retrieved from https://doi.org/10.1146/annurev.marine.010908.163855 (PMID: 21141663) doi: 10.1146/annurev.marine.010908.163855

Keppel, A. G., Breitburg, D. L., & Burrell, R. B. (2016, 08). Effects of co-varying diel-cycling hypoxia and ph on growth in the juvenile eastern oyster, crassostrea virginica. *PLOS ONE*, *11*(8), 1-31. Retrieved from https://doi.org/10.1371/journal.pone.0161088 doi: 10.1371/journal.pone.0161088

Kolodziejczyk, N., Testor, P., Lazar, A., Echevin, V., Krahmann, G., Chaigneau, A., ... Karstensen, J. (2018). Subsurface fine-scale patterns in an anticyclonic eddy off cap-vert peninsula observed from glider measurements. *Journal of Geophysical Research: Oceans*, *123*(9), 6312-6329. Retrieved from https://agupubs.onlinelibrary.wiley.com/doi/abs/10.1029/2018JC014135 doi: https://doi.org/10.1029/2018JC014135

Kopte, R., Brandt, P., Dengler, M., Tchipalanga, P. C. M., Macuria, M., & Ostrowski, M. (2017). The angola current: Flow and hydrographic characteristics as observed at 11s. *Journal of Geophysical Research: Oceans*, *122*(2), 1177-1189. Retrieved from https://agupubs.onlinelibrary.wiley.com/doi/abs/10.1002/2016JC012374 doi: https://doi.org/10.1002/2016JC012374

Kostianoy, A. G., & Lutjeharms, J. R. E. (1999). Atmospheric effects in the angola-benguela frontal zone. *Journal of Geophysical Research: Oceans*, *104*(C9), 20963-20970. Retrieved from https://agupubs.onlinelibrary.wiley.com/doi/abs/10.1029/1999JC900017 doi: https://doi.org/10.1029/1999JC900017

Liu, J., Emery, W. J., Wu, X., Li, M., Li, C., & Zhang, L. (2017). Computing coastal ocean surface currents from modis and viirs satellite imagery. *Remote Sensing*, *9*(10). Retrieved from https://www.mdpi.com/2072-4292/9/10/

1083 doi: 10.3390/rs9101083

Löscher, C. R., Bange, H. W., Schmitz, R. A., Callbeck, C. M., Engel, A., Hauss, H., ... Wagner, H. (2016). Water column biogeochemistry of oxygen minimum zones in the eastern tropical north atlantic and eastern tropical south pacific oceans. *Biogeosciences*, *13*(12), 3585–3606. Retrieved from https://bg.copernicus.org/articles/13/3585/2016/ doi: 10.5194/bg-13-3585-2016

Mackas, D. L., Strub, P. T., Thomas, A., & Montecino, V. (2006). Eastern ocean boundaries, pan-regional overview. In A. R. Robinson & K. Brink (Eds.), *The sea, volume 14: The global coastal ocean* (chap. 2). Harvard University Press.

Madec, G., & Team, N. S. (n.d.). Nemo ocean engine (Computer software manual No. 27). Zenodo. doi: 10.5281/zenodo.1464816

McCoy, D., Bianchi, D., & Stewart, A. L. (2020). Global observations of submesoscale coherent vortices in the ocean. *Progress in Oceanography*, *189*, 102452. Retrieved from https://www.sciencedirect.com/science/article/pii/S0079661120301890 doi: https://doi.org/10.1016/j.pocean.2020.102452

McDougall, T., & Barker, P. (2011). *Getting started with teos-10 and the gibbs seawater (gsw) oceanographic toolbox, 28pp., scor/iapso wg127* (Tech. Rep.). Retrieved from http://www.teos-10.org ((Accessed: 08 September 2021))

McGillicuddy, D. J. (2016). Mechanisms of physical-biological-biogeochemical interaction at the oceanic mesoscale. *Annual Review of Marine Science*, *8*, 125-159. doi: 10.1146/annurev-marine-010814-015606

Merckelbach, L., Smeed, D., & Griffiths, G. (2010). Vertical water velocities from underwater gliders. *Journal of Atmospheric and Oceanic Technology*, *27*(3), 547 - 563. Retrieved from https://journals.ametsoc.org/view/journals/atot/27/3/2009jtecho710_1.xml doi: 10.1175/2009JTECHO710.1

Messié, M., Ledesma, J., Kolber, D. D., Michisaki, R. P., Foley, D. G., & Chavez, F. P. (2009). Potential new production estimates in four eastern boundary upwelling ecosystems. *Progress in Oceanography*, *83*(1), 151-158. Retrieved from https://www.sciencedirect.com/science/article/pii/S0079661109000731 (Eastern Boundary Upwelling Ecosystems: Integrative and Comparative Approaches) doi: https://doi.org/10.1016/j.pocean.2009.07.018

Mohrholz, V., Bartholomae, C., van der Plas, A., & Lass, H. (2008). The seasonal variability of the northern benguela undercurrent and its relation to the oxygen budget on the shelf. *Continental Shelf Research*, *28*(3), 424-441. Retrieved from https://www.sciencedirect.com/science/article/pii/S0278434307002944 doi: https://doi.org/10.1016/j.csr.2007.10.001

Mohrholz, V., Eggert, A., Junker, T., Nausch, G., Ohde, T., & Schmidt, M. (2014). Cross shelf hydrographic and hydrochemical conditions and their short term variability at the northern benguela during a normal upwelling season. *Journal of Marine Systems*, *140*, 92-110. Retrieved from https://www.sciencedirect.com/science/article/pii/S0924796314001055 (Upwelling Ecosystem Succession) doi: https://doi.org/10.1016/j.jmarsys.2014.04.019

Molemaker, M. J., McWilliams, J. C., & Dewar, W. K. (2015). Submesoscale instability and generation of mesoscale anticyclones near a separation of the california undercurrent. *Journal of Physical Oceanography*, *45*(3), 613 - 629. Retrieved from https://journals.ametsoc.org/view/journals/phoc/45/3/jpo-d-13-0225.1.xml doi: 10.1175/JPO-D-13-0225.1

Monteiro, P., van der Plas, A., Mélice, J.-L., & Florenchie, P. (2008). Interannual hypoxia variability in a coastal upwelling system: Oceanshelf exchange, climate and ecosystem-state implications. *Deep Sea Research Part I: Oceanographic Research Papers*, *55*(4), 435-450. Retrieved from https://www.sciencedirect.com/science/article/pii/S0967063707002622 doi: https://doi.org/10.1016/j.dsr.2007.12.010

Monteiro, P., van der Plas, A., Mohrholz, V., Mabille, E., Pascall, A., & Joubert, W. (2006). Variability of natural hypoxia and methane in a coastal upwelling system: Oceanic physics or shelf biology? *Geophysical Research Letters*, *33*(16). Retrieved from https://agupubs.onlinelibrary.wiley.com/doi/abs/10.1029/2006GL026234 doi: https://doi.org/10.1029/2006GL026234

Muller, A., Reason, C., Schmidt, M., Mohrholz, V., & Eggert, A. (2014). Computing transport budgets along the shelf and across the shelf edge in the northern benguela during summer (djf) and winter (jja). *Journal of Marine Systems*, *140*, 82-91. Retrieved from https://www.sciencedirect.com/science/article/pii/S0924796314000360 (Upwelling Ecosystem Succession) doi: https://doi.org/10.1016/j.jmarsys.2014.02.007

NASA-OBPG. (2018a). *Moderate-resolution imaging spectroradiometer (modis) aqua ocean color data* (Tech. Rep.). NASA Goddard Space Flight Center, Ocean Ecology Laboratory, Ocean Biology Processing Group, NASA OB.DAAC, Greenbelt, MD, USA. Retrieved from https://oceancolor.gsfc.nasa.gov/data/10.5067/AQUA/MODIS/L2/OC/2018/(Lastaccessedon20/06/2022) (2018 Reprocessing) doi: 10.5067/AQUA/MODIS/L2/OC/2018

NASA-OBPG. (2018b). *Moderate-resolution imaging spectroradiometer (modis) terra ocean color data* (Tech. Rep.). NASA Goddard Space Flight Center, Ocean Ecology Laboratory, Ocean Biology Processing Group, NASA OB.DAAC, Greenbelt, MD, USA. Retrieved from https://oceancolor.gsfc.nasa.gov/data/10.5067/TERRA/MODIS/L2/OC/2018/(Lastaccessedon20/06/2022) (2018 Reprocessing) doi: 10.5067/TERRA/MODIS/L2/OC/2018

NASA-OBPG. (2018c). *Visible and infrared imager/radiometer suite (viirs) ocean color data* (Tech. Rep.). NASA Goddard Space Flight Center, Ocean Ecology Laboratory, Ocean Biology Processing Group. Retrieved from https://oceancolor.gsfc.nasa.gov/data/10.5067/JPSS1/VIIRS/L2/OC/2018/(Lastaccessedon20/06/2022) (2018 Reprocessing) doi: 10.5067/JPSS1/VIIRS/L2/OC/2018

NOAA data set. (2018). *World ocean atlas 2018 (woa18).* (Available at: https://www.ncei.noaa.gov/data/oceans/woa/WOA18/DATA/ (Accessed: 19 January 2021))

Ohde, T., & Dadou, I. (2018). Seasonal and annual variability of coastal sulphur plumes in the northern benguela upwelling system. *PloS one*, *13*(2), e0192140.

Pawlowicz, R. (2020). *M_map: A mapping package for matlab* (Tech. Rep.). Retrieved from www.eoas.ubc.ca/~rich/map.html (version 1.4m)

Pitcher, G. C., Aguirre-Velarde, A., Breitburg, D., Cardich, J., Carstensen, J., Conley, D. J., ... Zhu, Z. (2021). System controls of coastal and open ocean oxygen depletion. *Progress in Oceanography*, *197*, 102613. Retrieved from https://www.sciencedirect.com/science/article/pii/S0079661121001002 doi: https://doi.org/10.1016/j.pocean.2021.102613

Poole, R., & Tomczak, M. (1999). Optimum multiparameter analysis of the water mass structure in the atlantic ocean thermocline. *Deep Sea Research Part I: Oceanographic Research Papers*, *46*(11), 1895-1921. Retrieved from https://www.sciencedirect.com/science/article/pii/S0967063799000254 doi: https://doi.org/10.1016/S0967-0637(99)00025-4

Rio, M.-H., Mulet, S., & Picot, N. (2014). Beyond goce for the ocean circulation estimate: Synergetic use of altimetry, gravimetry, and in situ data provides new insight into geostrophic and ekman currents. *Geophysical Research Letters*, *41*(24), 8918–8925.

Rouault, M. (2012). Bi-annual intrusion of tropical water in the northern benguela upwelling. *Geophysical Research Letters*, *39*(12). Retrieved from https://agupubs.onlinelibrary.wiley.com/doi/abs/10.1029/2012GL052099 doi: https://doi.org/10.1029/2012GL052099

Rouault, M., Illig, S., Bartholomae, C., Reason, C., & Bentamy, A. (2007). Propagation and origin of warm anomalies in the angola benguela upwelling system in 2001. *Journal of Marine Systems*, *68*(3), 473-488. Retrieved from https://www.sciencedirect.com/science/article/pii/S0924796306003538 doi: https://doi.org/10.1016/j.jmarsys.2006.11.010

Sanders, R. J., Henson, S. A., Martin, A. P., Anderson, T. R., Bernardello, R., Enderlein, P., ... Zubkov, M. (2016). Controls over ocean mesopelagic interior carbon storage (comics): Fieldwork, synthesis, and modeling efforts. *Frontiers in Marine Science*, *3*, 136. Retrieved from https://www.frontiersin.org/article/10.3389/fmars.2016.00136 doi: 10.3389/fmars.2016.00136

Sarmiento, J. L., & Gruber, N. (2006). *Ocean biogeochemical dynamics*. Princeton University Press. (ISBN: 9781400849079)

Schmidt, M., & Eggert, A. (2016). Oxygen cycling in the northern benguela upwelling system: Modelling oxygen sources and sinks. *Progress in Oceanography*, *149*, 145-173. Retrieved from https://www.sciencedirect.com/science/article/pii/S0079661116301975 doi: https://doi.org/10.1016/j.pocean.2016.09.004

Schmidtko, S., Stramma, L., & Visbeck, M. (2017). Decline in global oceanic oxygen content during the past five decades. *Nature*, *542*(7641), 335–339.

Schütte, F., Brandt, P., & Karstensen, J. (2016a). Occurrence and characteristics of mesoscale eddies in the tropical northeastern atlantic ocean. *Ocean Science*, *12*(3), 663–685. Retrieved from https://www.ocean-sci.net/12/663/2016/ doi: 10.5194/os-12-663-2016

Schütte, F., Frenger, I., Burmeister, K., Speich, S., & Karstensen, J. (EGU2021, talk). Does the interior of the ocean hide a major part of the eddy field? *EGU General Assembly 2021*, online conference, 1930 Apr 2021. Retrieved from https://doi.org/10.5194/egusphere-egu21-8880 doi: 10.5194/egusphere-egu21-8880

Schütte, F., Karstensen, J., Krahmann, G., Hauss, H., Fiedler, B., Brandt, P., ... Körtzinger, A. (2016b). Characterization of "dead-zone" eddies in the eastern tropical north atlantic. *Biogeosciences*, *13*(20), 5865–5881. Retrieved from https://www.biogeosciences.net/13/5865/2016/ doi: 10.5194/bg-13-5865-2016

Shannon, L. V., Agenbag, J. J., & Buys, M. E. L. (1987). Large- and mesoscale features of the angola-benguela front. *South African Journal of Marine Science*, *5*(1), 11-34. Retrieved from https://doi.org/10.2989/025776187784522261 doi: 10.2989/025776187784522261

Siegfried, L., Schmidt, M., Mohrholz, V., Pogrzeba, H., Nardini, P., Bttinger, M., & Scheuermann, G. (2019, 01). The tropical-subtropical coupling in the southeast atlantic from the perspective of the northern benguela upwelling system. *PLOS ONE*, *14*(1), 1-31. Retrieved from https://doi.org/10.1371/journal.pone.0210083 doi: 10.1371/journal.pone.0210083

SLOCUM manual. (2017). *Slocum g3 glider operators manual* (Tech. Rep.). Teledyne Webb Research. Retrieved from http://gliderfs.coas.oregonstate.edu/gliderweb/docs/slocum_manuals/Slocum_G3_Operator_Manual_20171219.pdf (Accessed: 30 September 2021)

Sowman, M., & Cardoso, P. (2010). Small-scale fisheries and food security strategies in countries in the benguela current large marine ecosystem (bclme) region: Angola, namibia and south africa. *Marine Policy*, *34*(6), 1163-1170. Retrieved from https://www.sciencedirect.com/science/article/pii/S0308597X10000680 doi: https://doi.org/10.1016/j.marpol.2010.03.016

Stramma, L., & England, M. (1999). On the water masses and mean circulation of the south atlantic ocean. *Journal of Geophysical Research: Oceans*, *104*(C9), 20863-20883. Retrieved from https://agupubs.onlinelibrary.wiley.com/doi/abs/10.1029/1999JC900139 doi: https://doi.org/10.1029/

1999JC900139

Stramma, L., Johnson, G. C., Sprintall, J., & Mohrholz, V. (2008). Expanding oxygen-minimum zones in the tropical oceans. *Science*, *320*(5876), 655–658. Retrieved from https://science.sciencemag.org/content/320/5876/655 doi: 10.1126/science.1153847

Sullivan, J. M., Twardowski, M. S., Ronald, J., Zaneveld, V., & Moore, C. C. (2013). Measuring optical backscattering in water. In *Light scattering reviews 7: Radiative transfer and optical properties of atmosphere and underlying surface* (pp. 189–224). Berlin, Heidelberg: Springer Berlin Heidelberg. Retrieved from https://doi.org/10.1007/978-3-642-21907-8_6 doi: 10.1007/978-3-642-21907-8_6

Tchipalanga, P., Dengler, M., Brandt, P., Kopte, R., Macuria, M., Coelho, P., ... Keenlyside, N. S. (2018). Eastern boundary circulation and hydrography off angola: Building angolan oceanographic capacities. *Bulletin of the American Meteorological Society*, *99*(8), 1589 - 1605. Retrieved from https://journals.ametsoc.org/view/journals/bams/99/8/bams-d-17-0197.1.xml doi: 10.1175/BAMS-D-17-0197.1

Thomsen, S., Kanzow, T., Colas, F., Echevin, V., Krahmann, G., & Engel, A. (2016). Do submesoscale frontal processes ventilate the oxygen minimum zone off peru? *Geophysical Research Letters*, *43*(15), 8133-8142. Retrieved from https://agupubs.onlinelibrary.wiley.com/doi/abs/10.1002/2016GL070548 doi: https://doi.org/10.1002/2016GL070548

Thomsen, S., Kanzow, T., Krahmann, G., Greatbatch, R. J., Dengler, M., & Lavik, G. (2016). The formation of a subsurface anticyclonic eddy in the peru-chile undercurrent and its impact on the near-coastal salinity, oxygen, and nutrient distributions. *Journal of Geophysical Research: Oceans*, *121*(1), 476-501. Retrieved from https://agupubs.onlinelibrary.wiley.com/doi/abs/10.1002/2015JC010878 doi: https://doi.org/10.1002/2015JC010878

Vaquer-Sunyer, R., & Duarte, C. M. (2008). Thresholds of hypoxia for marine biodiversity. *Proceedings of the National Academy of Sciences*, *105*(40), 15452–15457. Retrieved from https://www.pnas.org/content/105/40/15452 doi: 10.1073/pnas.0803833105

Veitch, J. A., Florenchie, P., & Shillington, F. A. (2006). Seasonal and interannual fluctuations of the angolabenguela frontal zone (abfz) using 4.5 km resolution satellite imagery from 1982 to 1999. *International Journal of Remote Sensing*, *27*(5), 987-998. Retrieved from https://doi.org/10.1080/01431160500127914 doi: 10.1080/01431160500127914

Wyrtki, K. (1962). The oxygen minima in relation to ocean circulation. In *Deep sea research and oceanographic abstracts* (Vol. 9, pp. 11–23).

Zhang, J., Gilbert, D., Gooday, A. J., Levin, L., Naqvi, S. W. A., Middelburg, J. J., ... Van der Plas, A. K. (2010). Natural and human-induced hypoxia and consequences for coastal areas: synthesis and future development. *Biogeosciences*, *7*(5), 1443–1467. Retrieved from https://bg.copernicus.org/articles/7/1443/2010/ doi: 10.5194/bg-7-1443-2010